交通部中央氣象局委託研究計畫成果報告

月、季定量降水預報技術之研發與應用

計畫類別：■國內　　□國外

計畫編號：MOTC-CWB-96-6M-03

執行期間：　96 年　2 月 16 日至　96 年　12 月　31 日

計畫主持人：陳正達

執行單位：氣象應用推廣基金會

中華民國　　96 年　12 月　5 日

交通部中央氣象局　年度政府部門科技計畫期末摘要報告

計畫名稱：

審議編號：		部會署原計畫編號：	MOTC-CWB-96-6M-03
主管機關：	交通部中央氣象局	執行單位：	氣象應用推廣基金會
計畫主持人：	陳正達	聯絡人：	黃美鳳
電話號碼：	(02)29309545	傳真號碼：	(02)29333315
期程：	96 年 2 月 16 日　至　96 年 12 月 31 日		
經費：(全程)	2400 仟元	經費(年度)	2400 仟元

執行情形：

1.執行進度：

	預定（%）	實際（%）	比較（%）
當年全程	100	100	0

2.經費支用：

	預定	實際	支用率（%）
當年全程	2,400,000	2,400,000	100

3.主要執行成果：

a. 整合計畫相關學術單位以及氣象局模式的模擬與預報結果，每個月持續以已建立的二階段、多假想海溫、多重模式動力氣候預報系統（參見圖一）進行全球與區域的月季降雨預報實驗，提供作為長期預報科的實際預報參考。本年度延續過去工作重點，將進一步分析個別與多重模式於 1981-2003 年期間，起始於 2、5、8、11 月的歷史預報（hindcast）的 10 個系集成員資料，除了以美國 NCEP CFS 預報海溫，驅動不同大氣環流模式的模擬預報工作外，部份模式也將以中央氣象局發展的動力統計海溫預報（OPGSST）驅動

模式。模式驗證評估工作則是依據世界氣象組織制定的長期預報標準化驗證架構（參見表一）。

b. 延續之前的三分類降雨距平預報（偏多、正常、偏少；30%—40%—30%）外，本年度的分析重點之一是，針對更極端季節降雨距平的預報技術進行客觀評估，計畫所選擇的極端季節降雨是以 80 與 20 百分位作為極多與極少的判定標準，雖然不是非常極端的事件，可是以二十幾年的歷史預報而言，也很難處理更為極端的部份，而且也與目前英國氣象局的做法一致。此外，也進一步以敏感度測試的方式，比較以 85 與 15 百分位為極多與極少的判定標準時的差異，或者回歸近似兩分類（只有偏多與偏少）的 45 與 55 百分位為基準時的機率預報的預報技術。

c. 本年度的另外一個新的研究方向是研究季節預報的潛在經濟價值，在此我們會先透過簡單的二分類列聯表（Contengency table）以及準備代價與損失的比值（cost/loss ratio），分析目前所建立的預報系統，對季節降雨偏多與偏少兩類預報的相對價值（ $V=(E_{climate}-E_{forecast})/((E_{climate}-E_{perfect})$ ）隨著不同準備代價與損失比值的變化情形，不同的下游應用單位可以自行估計其對於季節降雨偏多與偏少的預報所衍生的潛在相對價值。

d. 今年四月初，由計畫主持人與其博士班學生朱容練前往位於韓國釜山的APEC 氣候中心，進行交流訪問並針對與中央氣象局在月、季氣候預報的合作計畫交換意見，APEC 氣候中心現階段已是頗具規模的氣候預報中心，在開發多模式系集預報技術方面有相當優異的表現，參與的 APEC 國家與氣候模式眾多，中央氣象局也是正式的成員之一，將透過計畫加強中央氣象局與其之互動，及預報資料交換與經驗交流。訪問期間計畫主持人以專題演講報告與討論目前計畫所建構的預報系統與歷史預報的驗證與評估，博士班學生朱容練則進一步在 APEC 氣候中心進行長期的研究訪問，針對雙方都有興趣的降雨月季預報統計降尺度問題，提出具體的方法並評估其準確率。目前已經發展出一套具體的方法，相關的結果已經撰寫為期刊論文（參見報告最後之附件），即將在小幅修正後，刊載於 JGR-Atmosphere，此工作也具體與 APEC 的研究人員有緊密的合作，APEC 氣候中心主任 Dr. C.-K. Park 也對其表現極為讚賞，為未來氣象局更積極參與 APEC 氣候中心，建立良好的基礎。

4. 計畫變更說明：

計畫內容未變更。

5. 落後原因：

計畫進度並未落後，在歷史預報（hindcast）實驗進行部份，各執行單位已完

成 1981-2003 年期間，運用美國 NCEP CFS 預報海溫驅動，起始於 2、5、8、11 月的兩個季節、10 個成員的系集預報，部份模式並進一步以中央氣象局發展的動力統計海溫預報(OPGSST)重複上述系集預報，並進行預報驗證工作。在其他預報起始月份方面，少數模式將繼續逐步建立更完整的歷史預報資料，不過這部份並不在預計完成的部份。

6.主管機關之因應對策（檢討與建議）：

本年度各參與預報系統的執行學校單位，並沒有設備租賃採購之費用，但已積極協調各執行單位，運用各執行單位現有計算與資料儲存資源，支援計劃所需。

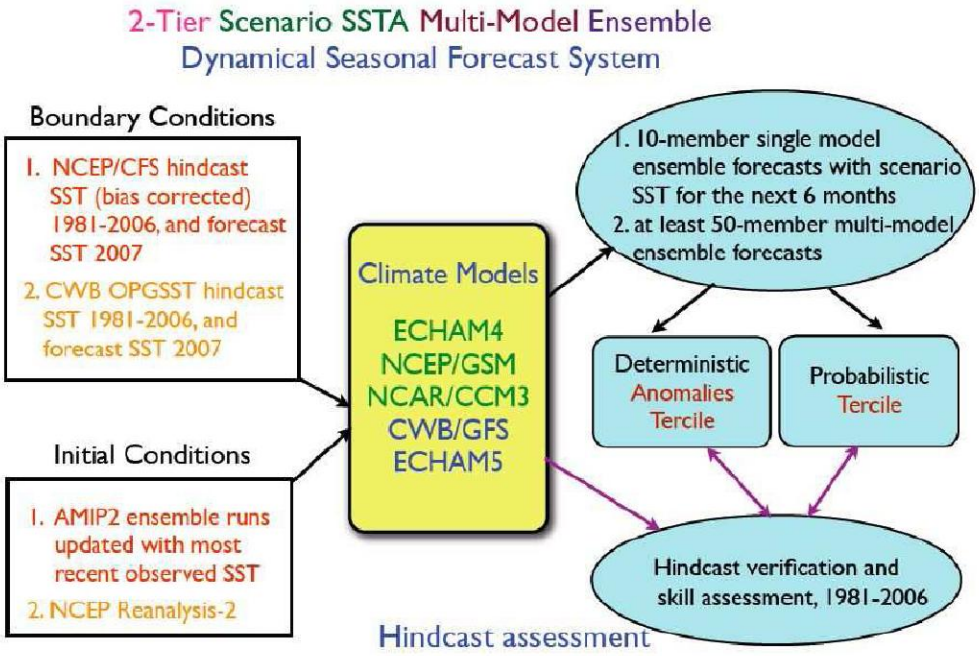

圖一、二階段、多假想海溫、多重模式系集動力預報系統以及驗證、評估、誤差修正方法架構示意圖

世界氣象組織制定的長期預報標準化驗證架構

Parameter	Verification regions	Deterministic Forecasts	Probabilistic Forecasts
Level 1 : Large scale aggregated overall measures of forecast performance			
Precipitation anomaly	Tropics Northern Extra-Tropics Southern Extra-Tropics (East Asia)	MSSS (bulk number)	ROC curves ROC areas Reliability diagrams Frequency histograms
Level 2:Verification at grid points			
Precipitation anomaly	grid point verification on a 2.5° by 2.5° grid	1. MSSS and its three term decomposition at each grid point 2. number of forecast- observation pairs 3. mean of observations and forecasts 4. variance of observations and forecasts 5. correlation of forecasts and observations	ROC areas at each grid point in graphic representation
Level3: Grid point by grid point contingency tables for more extensive verification			
Precipitation anomaly	grid point verification on a 2.5° by 2.5° grid	3 by 3 contingencytables at each grid point Gerrity Skill Score	ROC reliability tables at each grid point

表一、 世界氣象組織制定的長期預報標準化驗證架構表。

月、季定量降水預報技術之研發與應用

執行單位：財團法人氣象應用推廣基金會　　計畫編號： MOTC-CWB-96-6M-03

計畫主持人：陳正達（國立台灣師範大學地球科學系教授）

計畫共同主持人：鄒治華（國立台灣師範大學地球科學系教授）

曾仁佑（國立中央大學大氣科學系副教授）

洪志誠（國立台北教育大學自然科學教育系副教授）

研究人員： 翁叔平、朱容練、吳郁娟、童裕翔、賈愛玫

聯絡方式：台北市汀州路 4 段 88 號　國立台灣師範大學地球科學系

E-mail: chen@rain.geos.ntnu.edu.tw

前言

月季時間尺度的降雨預報，目前已經是世界各個主要氣象預報作業中心在中長期預報工作的重點，近年來許多研究顯示，短期氣候預報的預報技術發展逐漸成熟，預報的特性也見有掌握，而這些預報的結果具有相當大的潛在社會經濟價值，有利政府與民間能在重大自然氣候變動（如旱澇與極端冷熱）發生前，儘早採取相關的因應措施。也因此，氣象局的中長期科技發展規劃之一，即是建立這種季節至年際尺度的區域氣候預報能力，並加以評估其預報特性與價值。在過去幾年，透過氣象局與大學的合作計畫，已經運用高速的叢集運算平台與數個全球氣候模式為主要的實驗預報基礎，以兩階段方式（two-tier approach）進行未來至少兩個季節的降雨氣候預報，並同時運用模式與觀測分析資料，進行個別與多重模式系集短期動力氣候的歷史模擬預報（hindcast），以世界氣象組織所制定的長期預報的標準化驗證程

序，做為驗證工作的準則，分別針對決定性與機率預報形式加以分析評估。本年度的計畫重點，除了持續進行、測試、擴展與測試已建立的多重模式實驗系集氣候預報系統之外，將同時運用美國環境預報中心的大氣海洋耦合預報系統（NCEP/CFS）與中央氣象局的動力統計預報系統（CWB/OPGSST）所預報的海溫距平，驅動此動力預報系統，以更完整地涵蓋海溫預報的不確定性所帶來的影響。此外也將進一步開始評估，除了三分類之外，更極端氣候事件的可預報度分析，並運用簡單的經濟模式，分析上述各種氣候預報產品在不同應用領域的潛在經濟效益。未來的預報產品將著重在客觀機率預報，以具體呈現預報的不確定特性，模擬與預報的結果將開放給相關研究與預報人員參考，並供下游應用、降尺度與風險評估社群善加利用。也同時可以協助氣象局積極參與 APEC 氣候中心的氣候預報相關活動，以充分運用區域共享的氣候預報資源，在亞太經合會（APEC）的架構下，推展區域的國際合作。

在過去的研究分析，比較德國馬克斯普朗克氣象研究所的 ECHAM4.6 與 ECHAM5.2 模式、中央氣象局的全球大氣環流模式（CWB/GFS）、及美國大氣海洋總署環境預報中心的 NCEP/GSM、美國大氣科學研究中心的 NCAR/CCM3，從二、五、八、十一月起始的 1981 年至 2004 年的系集後報(Hindcast)實驗，並利用此五個模式進行多重模式系集預報的後報分析結果。結果顯示，在決定性三分類（偏多、正常、偏少）預報方面，GSS 技術得分在副熱帶海洋地區表現還算不錯，以春季和冬季特別是 ECHAM4、CWB/GFS、NCEP/GSM 和多重模式表現相對比較好；而在台灣地區一帶，冬季降水之 GSS 明顯比夏季和春季表現為佳。此外，本報告利用 ROC Curve 和 Reliability diagram 來驗證在決定性三分類（偏多、正常、偏少）機率預報結果；整體來說，多重超系集模式比個別模式有較好的降水表現，且冬季之 hindcast 降水比春季、夏季有更好的模擬結果。

本期計畫報告的重點，主要是針對極端月季降雨距平的預報技術與過去基本三分類預報的比較，所問的問題是，極端月季降雨距平（如果定義為 20 百分位以下為極少或 80 百分位以上為極多）是否比一般三分類預報（30-40-30%，偏少、正常、偏多）更好的表現呢？由於極端月季降雨距平無法直接用較適合整體總計的GSS技術得分加以評估，在此會以個別類別預報的Equitable Threat Score (ETS 或 Gilbert 技術得分)作為比較基準，在類別的機率預報方面則是著重於ROC score 與 Reliability Diagram（含 Brier Skill Score）的分析比較。 ROC score 還可以進一步檢視其分布及變化。

一、使用資料及評估方法

1.1 觀測資料

在觀測資料方面，本研究使用了全球降雨氣候計畫(Global Precipitation Climatology Project, GPCP)月平均降雨資料，水平解析度為 2.5 x 2.5 (將其差分至 T42)，資料長度為 1981 年 1 月到 2005 年 4 月，詳細資料內容，請參見 Huffman et al. (1997)。

1.2 模式資料

在模式資料方面，本研究以美國環境預報中心耦合預報系統(NCEP/CFS)的 Hindcast (後報)海溫預報資料，進行德國馬克斯普朗克氣象研究所的ECHAM4、中央氣象局的全球大氣模式(CWB/GFS)以及 ECHAM5、美國大氣研究中心的CCM3(NCAR/CCM3)、大氣海洋總署環境預報中心的NCEP/GSM，完成五個模式 2、5、8、11 月從 1981 年至 2004 年的系集後報(Hindcast)實驗。其

中每個模式均包括十個系集成員，水平解析度為三角截取 42 波(Triangular truncation 42 wavenumbers, T42)，對應東西方向 網格點，南北方向 64 個高斯網格點。選擇評估區域為東亞地區（80E-160E, EQ-50N)。此外 德國馬克斯普朗克氣象研究所的ECHAM4、中央氣象局的全球大氣模式(CWB/GFS)以及 ECHAM5 亦以中央氣象局的動力統計預報系統（CWB/OPGSST）所預報的海溫距平驅動，完成第二組假想海溫發展的系集後報(Hindcast)實驗，在多重模式組合的機率預報，是以上述八種模式與驅動海溫組合為基準。美國大氣海洋總署下的國家環境預報中心在 2004 年推出的大氣海洋耦合預報系統（NCEP/CFS）當作對應比較之一階段耦合模式。

1.3 評估方法

（1）Equitable Threat Score （ETS, Gilbert Skill Score）

ETS得分是評估觀測發生的分類事件有多少比例是被正確預報，但已調整了因隨機可能猜對的部份 （例如在下雨較多的地區比乾燥區更容易正確地預報降雨事件的發生），其計算公式如下：

ETS = (hits - hits_random) / (hits + misses + false alarms - hit_random)

其中 hits_random = (hits + misses)(hits + fasle alarms) / total

在此將比較以相對機率高低決定預報分類類別的ETS技術得分，在一般三分類時的偏多，以及以極端季節氣候降雨偏多的比較。

（2）Relative Operating Characteristics（ROC）curve 和 ROC scores

ROC是一個利用「命中預報」與「錯誤預報」比較下所得的技術得分，其中「命中預報HR_n」（Y軸）與「錯誤預報FAR_n」（X軸）的計算分別為：

$$HR_n = \frac{\sum_{i=n}^{N} O_i}{\sum_{i=1}^{N} O_i} \qquad FAR_n = \frac{\sum_{i=n}^{N} NO_i}{\sum_{i=1}^{N} NO_i} \text{。}$$

ROC scores 也是判定模式模擬結果的一個重要技術得分，其得分大小即為ROC的面積，最完美的技術得分為1，而當曲線剛好落在對角線時，此時技術得分（面積）即為0.5；ROC被用來做為模式技術得分的展現結果，而非判別與預報誤差之數據大小；偏差比較大的預報也許仍有好的ROC，因此ROC也可被視為是一種潛在效益的評量。

除了ROC技術得分外，也可利用curve來看模式模擬結果的表現。ROC curve的定義，一定要從座標（0,0）到（1,1），其值的範圍從0至1，當曲線向對角線左側彎曲時，表示「命中預報」大於「錯誤預報」；當ROC curve正好在對角線上時，此時為無預報技術；而當曲線在對角線之下時，亦即「命中預報」小於「錯誤預報」，則此預報技術低於隨機預報。不同於多數 skill score只能運用在決定性預報上，ROC則同時適用於決定性預報與機率預報。在本研究中，將資料以三分法區分（多雨、正常、少雨），並以此分類畫出三條ROC curve，藉此提供模式預報結果之可信度參考。

ROC score 的計算可以是整個宏觀區域的特性，也可以是個別網格點的值與分布情形。

（3）Reliability diagram 和Brier skill score

雖然ROC curve在小尺度上有比較高的感應，且一般人認為在長期預報上ROC curve比reliability diagram有更高的可信度，但為了讓模式在空間

分佈上能更加廣泛運用，利用較能考量大區域範圍的reliability diagrams輔助分析。Reliability diagram與ROC curve繪製原理相似，不過在X與Y軸所代表的，則是以預報機率範圍為條件下的觀測事件發生頻率；曲線可表示預報偏差，也可以更有效地判斷預報系統的特性，根據Wilks（1995）的分類，預報系統特性可以舉例如圖一中的子圖所示，其中圖a表現出的是氣候之展現值；而圖b展現出較小的resolution；圖c為曲線皆在對角線之上，表示預報出現underforecasting的偏差，反之，若曲線在對角線之下，表示預報overforecasting；而圖d為預報可信度表現出非常好的resolution；當reliability diagrams出現如e圖時，表示出此為一罕見的個案；最後若模式個案非常少，則呈現出的reliability diagrams則會類似 f 圖。在本研究中，將Reliability diagram結果與ROC互相搭配，作為提供預報是否接近真實的一個參考訊息。

圖一：Reliability and sharpness (from Wilks 1995)

此外，在本研究中，並提供Brier score (skill)的值協助Reliability diagram的判讀，並將結果與ROC互相搭配，作為提供預報是否接近真實的一個參考訊息。Brier score可視為趨勢預報中的mean square error，其最佳得分為0，BSS最佳得分為1；若BSS的值為0時，表示相對於參考預報是無預

報技術的。其中BS和BSS的計算如下：

（Brier score）$BS=\frac{1}{N}\sum_{i=1}^{N}\left(P_i-O_i\right)^2$

其中N為預報的總數，P_i為趨勢預報結果，O_i為實際觀測（計算過程中當事件發生時定義得分為1，事件未發生則得分為0），而上式可經轉換變為：

$$BS=\frac{1}{N}\sum_{i=1}^{N}\left(P_i-O_i\right)^2=\frac{1}{N}\sum_{K=1}^{T}n_K\left(P_K-\overline{O}_K\right)^2-\frac{1}{N}\sum_{K=1}^{T}n_K\left(\overline{O}_K-\overline{O}\right)^2+\overline{O}\left(1-\overline{O}\right)$$

Brier skill score：$BSS=\frac{BS-BS_{reference}}{0-BS_{reference}}=1-\frac{BS}{BS_{reference}}$

（4）Value Score

月季降雨預報對於不同的氣候資訊應用（例如期貨市場、水資源管理、公共衛生）而言，潛在的經濟效益與價值也有所差異，也因此比較好的方式是先以較普遍化的分析方式，不以特定的氣候資訊應用領域為限。計畫是採用David Richardson（2000）與Wilks（2001）所提出的方法，分別運用在季節降雨距平偏多與偏少的狀況加以分析。

Wilks (2001)

Protect?	Adverse Climate? Yes	Adverse Climate? No
Yes	Cost	Cost
No	Lost	0

Forecast event?	Observed event? Yes	Observed event? No
Yes	hits	false alarms
No	misses	

以上圖為例，當月季降雨距平偏多（或偏少）的情形發生時，如果不採取任何行動與調節措施時，假設會有一定的損失（Lost），但是採取調節與保護措施則需要一定的經費(Cost)，而同時對於月季降雨距平偏多與否，

是否可以被準確預報，可以計算預報的命中率（hits）、未預報率（misses）以及錯誤率（false alarms）的分布情形，將兩者結合便可以計算某一個預報系統所需的平均花費

E_forecast = F (1 - s) C - H s (L - C) + s L

F: false alarm rate, H: hit rate, s: base rate (frequency of observed events)

L: lost, C: cost

而價值得分（value score, V）的定義為

V = (E_climate - E_forecast) / (E_climate - E_perfect)

也就是一個預報系統的價值得分是，預報系統所獲得在平均花費的減低量相對於如果有完美預報時所可以獲得平均花費減低量。

當預報系統是完美時，決策人員只需要在觀測事件來臨時，才採取調節與保護措施，因此，E_perfect = s C。

E_climate (climate expense) 的估計比較複雜，如果決策人員不知道預報資訊，而決定不管如何總是採取調節與保護措施，那麼平均花費 E_always = C，反過來說，如果總是不採取調節與保護措施，那麼平均花費 E_never = s L，上述兩者未必相同，但決策人員應該試圖降低花費，而最佳的做法是，當 E_never > E_always 時，總是採取調節與保護措施；而 當 E_never < E_always 時，總是不採取調節與保護措施，所以以這種方式處理時，E_climate = minimum (C , s L)，將個別值帶入價值得分的定義，就可以估算之。

由於在上述情況下，價值得分（V）可以表示為 cost/loss 比值的函數，而不同的氣候應用範疇可以自行估算其準備代價與損失。

二、極端季節降雨預報結果評估

下列將以預報季節降雨距平的偏多（30%，左圖）與極多（20%，右圖）為例，比較多模式組合在不同起始月份（含 2, 5, 8, 11月）的各項技術得分。其他偏少與極少的情形，或者將極多（少）的條件改為15%時的敏感度測試，以及個別模式與不同預報領先時間等結果，可以至完整的計畫結果資料圖庫下載。

2.1 ETS 技術得分

以十一月起始，預報冬季（DJF）降雨距平的偏多（30%，左圖）與極多（20%，右圖）比較：

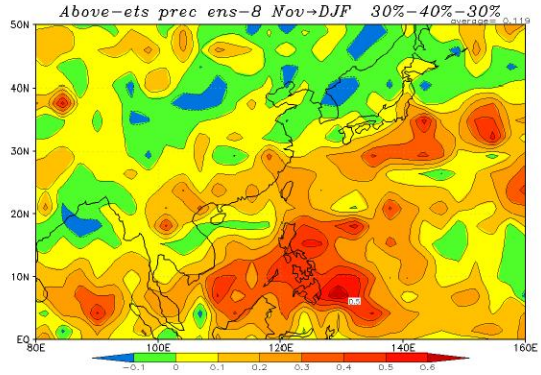

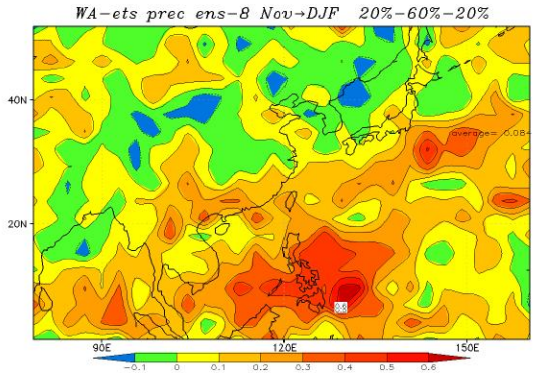

以二月起始，預報春季（MAM）降雨距平的偏多與極多比較：

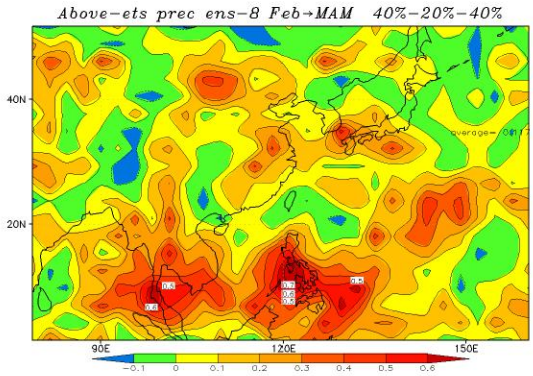

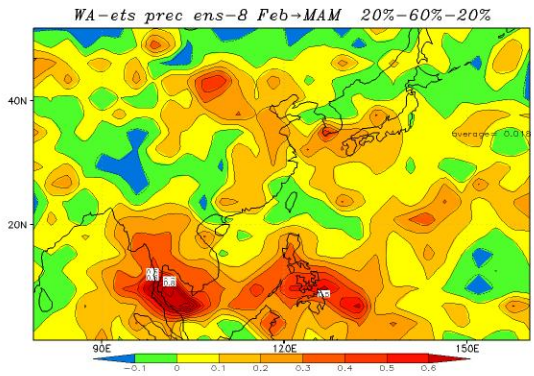

以五月起始，預報夏季（JJA）降雨距平的偏多與極多比較：

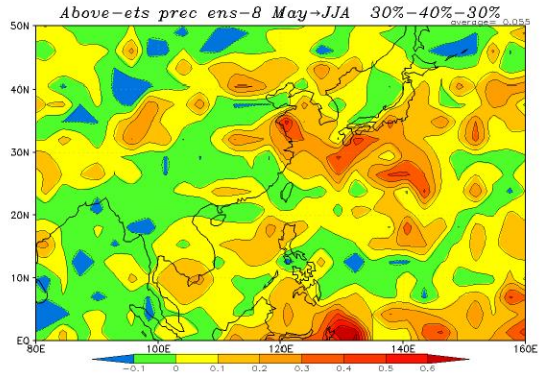

以八月起始，預報秋季（SON）降雨距平的偏多與極多比較：

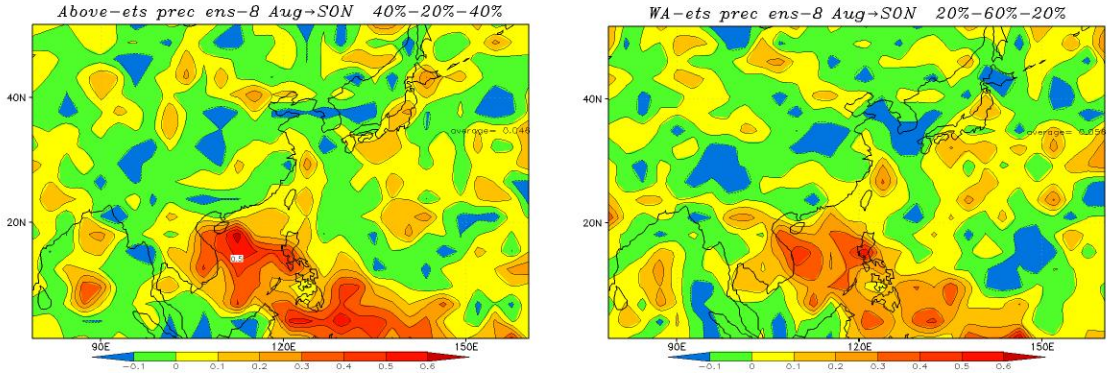

多模式組合在預報極多的機率預報所得的ETS score，一般而言，並不比三分類偏多的ETS score差。

2.2 ROC 技術得分

以十一月起始，預報冬季（DJF）降雨距平的偏多（30%，左圖）與極多（20%，右圖）的比較：

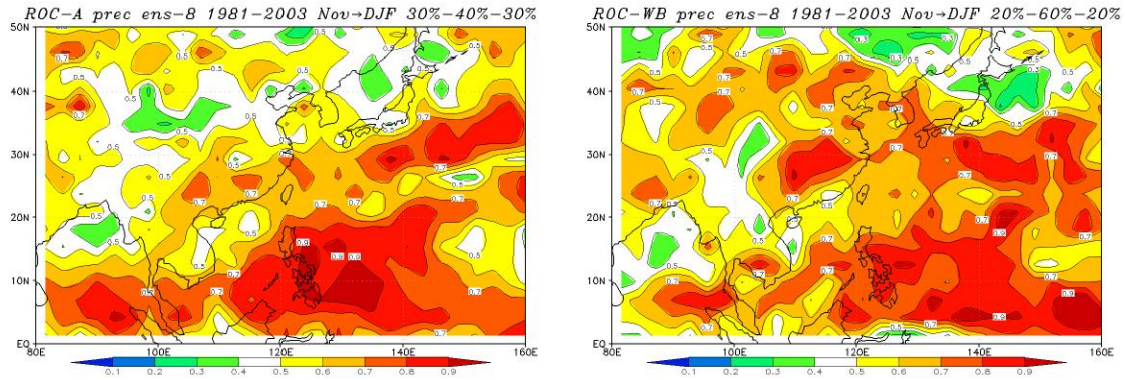

以二月起始，預報春季（MAM）降雨距平的偏多與極多比較：

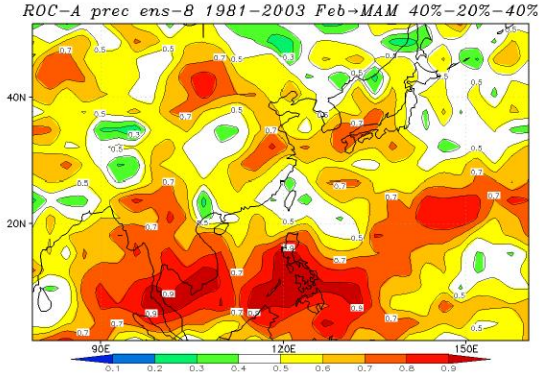

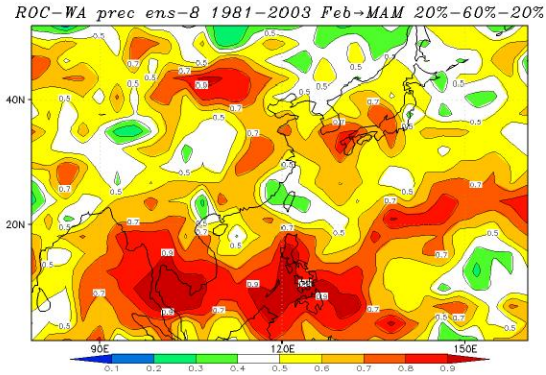

以五月起始，預報夏季（JJA）降雨距平的偏多與極多比較：

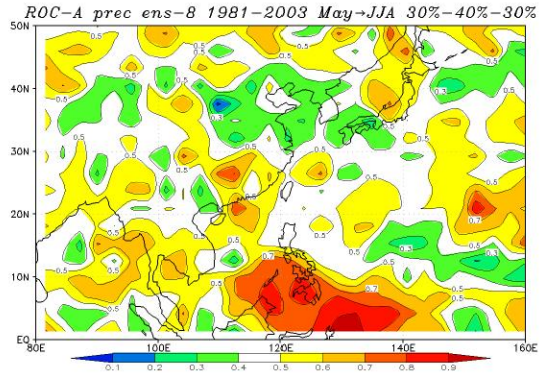

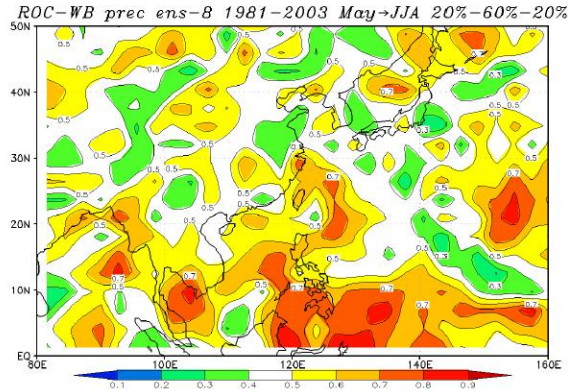

以八月起始，預報秋季（SON）降雨距平的偏多與極多比較：

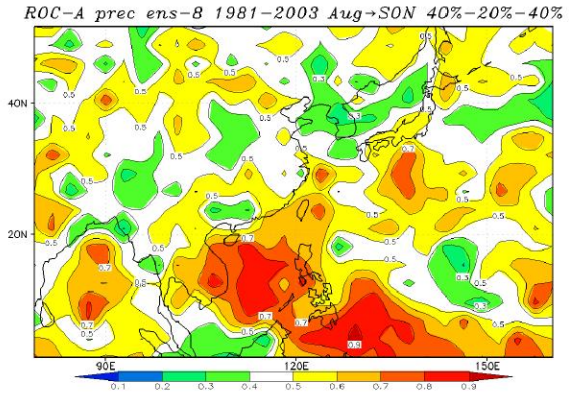

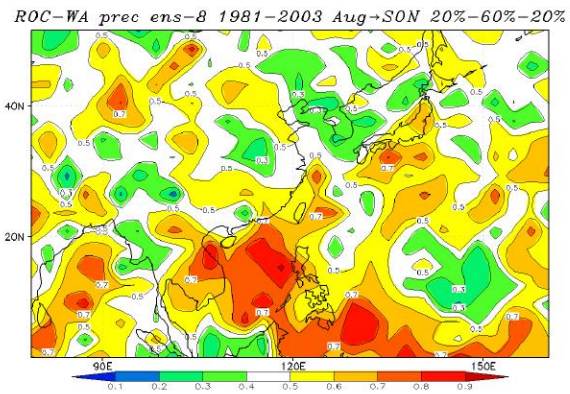

多模式組合在預報極多的機率預報所得的ROC score，一般而言，並不比三分類偏多的ROC score差。

2.3 Reliability Diagram and Brier Skill Score

以十一月起始，預報冬季（DJF）降雨距平的偏多（30%，左圖）與極多（20%，右圖）的比較，在此將個別模式的結果：

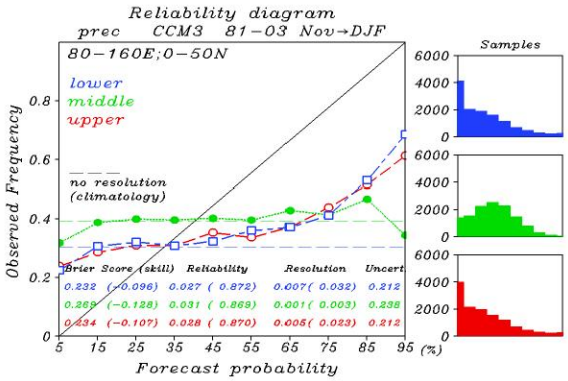
Reliability diagram
prec CCM3 81-03 Nov→DJF
80-160E;0-50N
lower
middle
upper
no resolution
(climatology)
Brier Score (skill) Reliability Resolution Uncert
0.232 (-0.096) 0.027 (0.872) 0.007(0.032) 0.212
0.269 (-0.128) 0.031 (0.869) 0.001(0.003) 0.238
0.234 (-0.107) 0.028 (0.870) 0.005(0.023) 0.212
Observed Frequency
Forecast probability
Samples

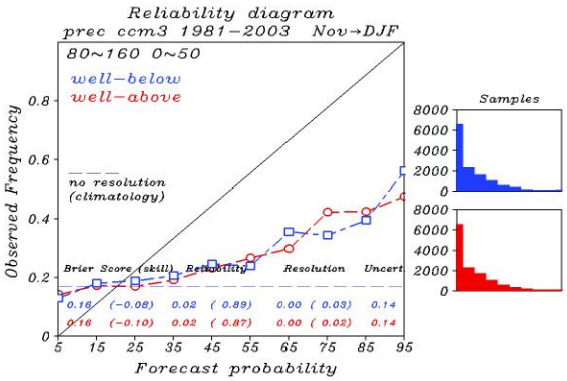
Reliability diagram
prec ccm3 1981-2003 Nov→DJF
80~160 0~50
well-below
well-above
no resolution
(climatology)
Brier Score (skill) Reliability Resolution Uncert
0.16 (-0.08) 0.02 (0.89) 0.00 (0.03) 0.14
0.16 (-0.10) 0.02 (0.87) 0.00 (0.02) 0.14
Observed Frequency
Forecast probability
Samples

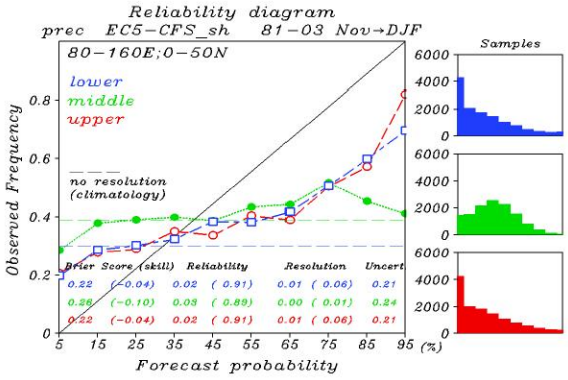
Reliability diagram
prec EC5-CFS_sh 81-03 Nov→DJF
80-160E;0-50N
lower
middle
upper
no resolution
(climatology)
Brier Score (skill) Reliability Resolution Uncert
0.22 (-0.04) 0.02 (0.91) 0.01 (0.06) 0.21
0.26 (-0.10) 0.03 (0.89) 0.00 (0.01) 0.24
0.22 (-0.04) 0.02 (0.91) 0.01 (0.06) 0.21
Observed Frequency
Forecast probability
Samples

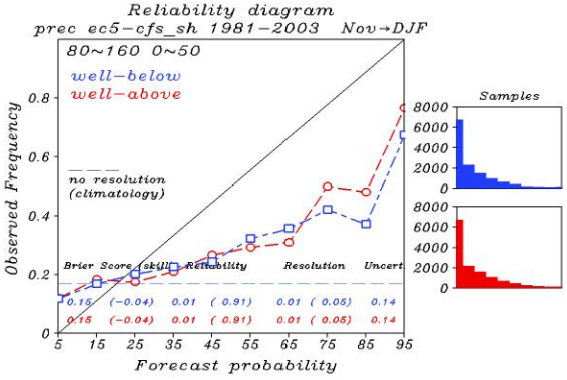
Reliability diagram
prec ec5-cfs_sh 1981-2003 Nov→DJF
80~160 0~50
well-below
well-above
no resolution
(climatology)
Brier Score (skill) Reliability Resolution Uncert
0.15 (-0.04) 0.01 (0.91) 0.01 (0.05) 0.14
0.15 (-0.04) 0.01 (0.91) 0.01 (0.05) 0.14
Observed Frequency
Forecast probability
Samples

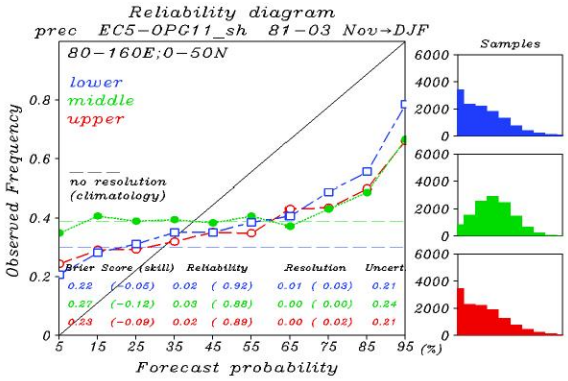
Reliability diagram
prec EC5-OPG11_sh 81-03 Nov→DJF
80-160E;0-50N
lower
middle
upper
no resolution
(climatology)
Brier Score (skill) Reliability Resolution Uncert
0.22 (-0.05) 0.02 (0.92) 0.01 (0.03) 0.21
0.27 (-0.12) 0.03 (0.88) 0.00 (0.00) 0.24
0.23 (-0.09) 0.02 (0.89) 0.00 (0.02) 0.21
Observed Frequency
Forecast probability
Samples

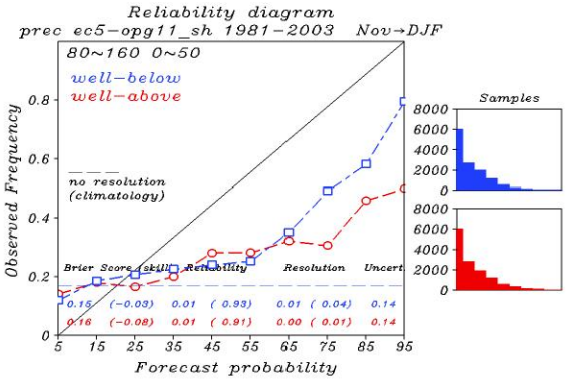
Reliability diagram
prec ec5-opg11_sh 1981-2003 Nov→DJF
80~160 0~50
well-below
well-above
no resolution
(climatology)
Brier Score (skill) Reliability Resolution Uncert
0.15 (-0.03) 0.01 (0.93) 0.01 (0.04) 0.14
0.16 (-0.08) 0.01 (0.91) 0.00 (0.01) 0.14
Observed Frequency
Forecast probability
Samples

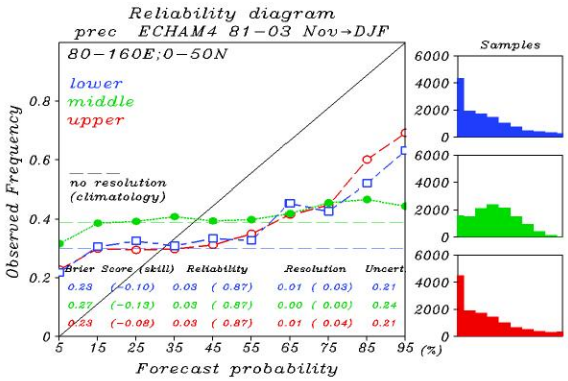
Reliability diagram
prec ECHAM4 81-03 Nov→DJF
80-160E;0-50N
lower
middle
upper
no resolution
(climatology)
Brier Score (skill) Reliability Resolution Uncert
0.23 (-0.10) 0.03 (0.87) 0.01 (0.03) 0.21
0.27 (-0.13) 0.03 (0.87) 0.00 (0.00) 0.24
0.23 (-0.08) 0.03 (0.87) 0.01 (0.04) 0.21
Observed Frequency
Forecast probability
Samples

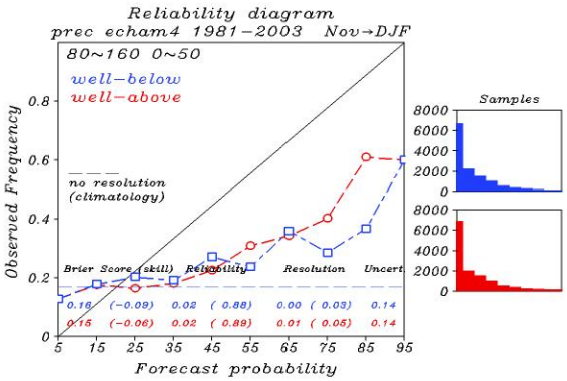
Reliability diagram
prec echam4 1981-2003 Nov→DJF
80~160 0~50
well-below
well-above
no resolution
(climatology)
Brier Score (skill) Reliability Resolution Uncert
0.16 (-0.09) 0.02 (0.88) 0.00 (0.03) 0.14
0.15 (-0.06) 0.02 (0.89) 0.01 (0.05) 0.14
Observed Frequency
Forecast probability
Samples

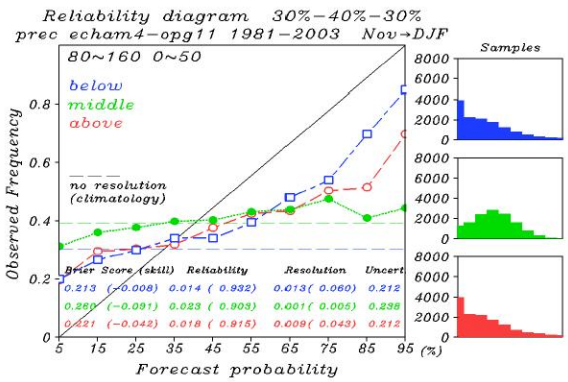
Reliability diagram 30%−40%−30%
prec echam4−opg11 1981−2003 Nov→DJF
80~160 0~50
below
middle
above
no resolution
(climatology)
Brier Score (skill) Reliability Resolution Uncert
0.213 (−0.008) 0.014 (0.932) 0.013(0.060) 0.212
0.260 (−0.091) 0.023 (0.903) 0.001(0.005) 0.238
0.221 (−0.042) 0.018 (0.915) 0.009(0.043) 0.212
Observed Frequency
Forecast probability
(%)
Samples

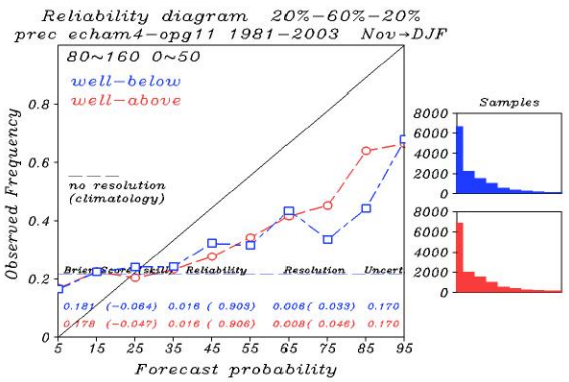
Reliability diagram 20%−60%−20%
prec echam4−opg11 1981−2003 Nov→DJF
80~160 0~50
well−below
well−above
no resolution
(climatology)
Brier Score (skill) Reliability Resolution Uncert
0.181 (−0.064) 0.016 (0.903) 0.008(0.033) 0.170
0.178 (−0.047) 0.016 (0.906) 0.008(0.046) 0.170
Observed Frequency
Forecast probability
Samples

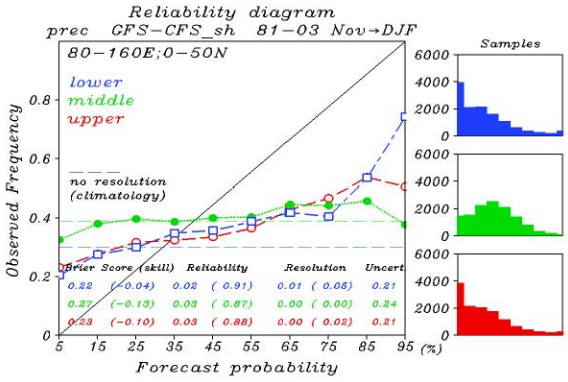
Reliability diagram
prec GFS−CFS_sh 81−03 Nov→DJF
80−160E;0−50N
lower
middle
upper
no resolution
(climatology)
Brier Score (skill) Reliability Resolution Uncert
0.22 (−0.04) 0.02 (0.91) 0.01 (0.05) 0.21
0.27 (−0.13) 0.03 (0.87) 0.00 (0.00) 0.24
0.23 (−0.10) 0.03 (0.88) 0.00 (0.02) 0.21
Observed Frequency
Forecast probability
(%)
Samples

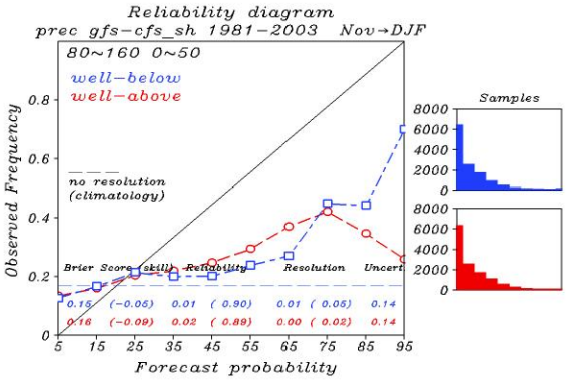
Reliability diagram
prec gfs−cfs_sh 1981−2003 Nov→DJF
80~160 0~50
well−below
well−above
no resolution
(climatology)
Brier Score (skill) Reliability Resolution Uncert
0.15 (−0.05) 0.01 (0.90) 0.01 (0.05) 0.14
0.16 (−0.09) 0.02 (0.89) 0.00 (0.02) 0.14
Observed Frequency
Forecast probability
Samples

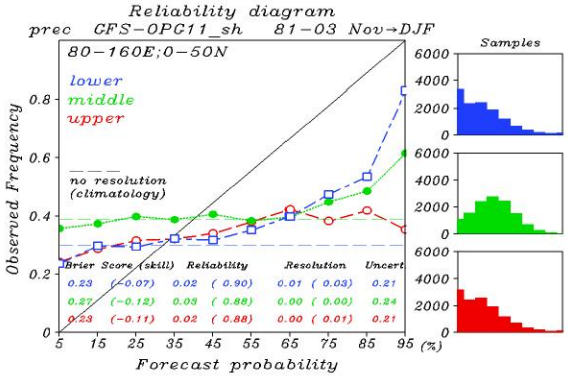
Reliability diagram
prec GFS−OPG11_sh 81−03 Nov→DJF
80−160E;0−50N
lower
middle
upper
no resolution
(climatology)
Brier Score (skill) Reliability Resolution Uncert
0.23 (−0.07) 0.02 (0.90) 0.01 (0.03) 0.21
0.27 (−0.12) 0.03 (0.88) 0.00 (0.00) 0.24
0.23 (−0.11) 0.02 (0.88) 0.00 (0.01) 0.21
Observed Frequency
Forecast probability
(%)
Samples

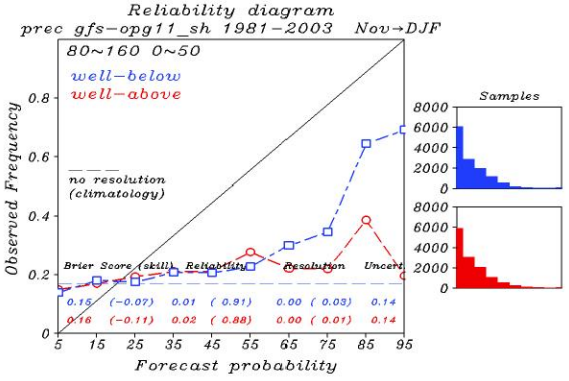
Reliability diagram
prec gfs−opg11_sh 1981−2003 Nov→DJF
80~160 0~50
well−below
well−above
no resolution
(climatology)
Brier Score (skill) Reliability Resolution Uncert
0.15 (−0.07) 0.01 (0.91) 0.00 (0.03) 0.14
0.16 (−0.11) 0.02 (0.88) 0.00 (0.01) 0.14
Observed Frequency
Forecast probability
Samples

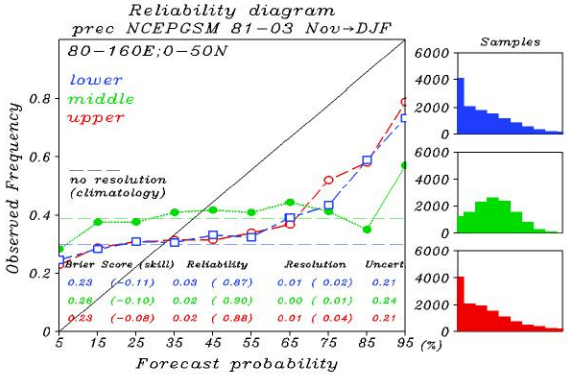
Reliability diagram
prec NCEPGSM 81−03 Nov→DJF
80−160E;0−50N
lower
middle
upper
no resolution
(climatology)
Brier Score (skill) Reliability Resolution Uncert
0.23 (−0.11) 0.03 (0.87) 0.01 (0.02) 0.21
0.26 (−0.10) 0.02 (0.90) 0.00 (0.01) 0.24
0.23 (−0.08) 0.02 (0.88) 0.01 (0.04) 0.21
Observed Frequency
Forecast probability
(%)
Samples

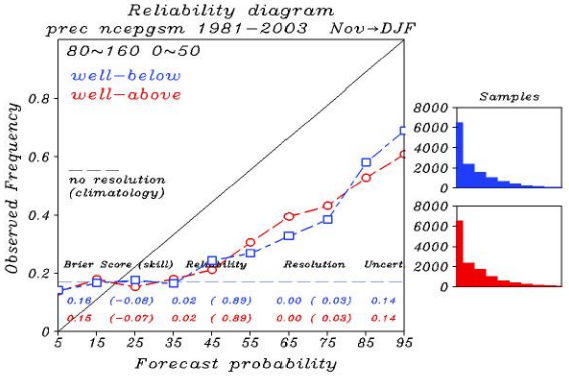
Reliability diagram
prec ncepgsm 1981−2003 Nov→DJF
80~160 0~50
well−below
well−above
no resolution
(climatology)
Brier Score (skill) Reliability Resolution Uncert
0.16 (−0.08) 0.02 (0.89) 0.00 (0.03) 0.14
0.15 (−0.07) 0.02 (0.89) 0.00 (0.03) 0.14
Observed Frequency
Forecast probability
Samples

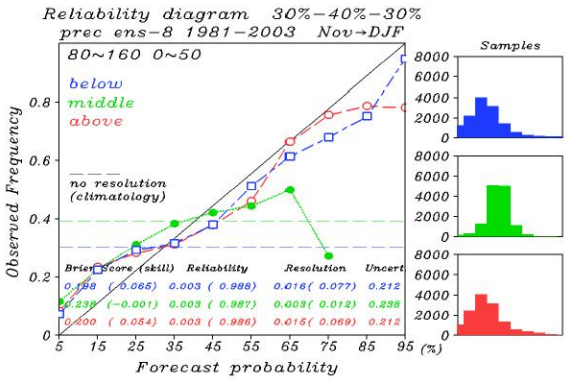

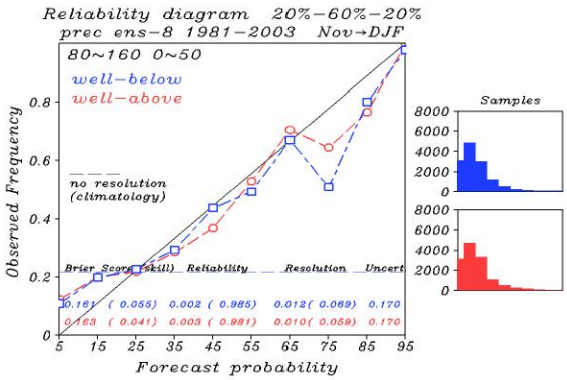

以二月起始，預報春季（MAM）降雨距平的偏多與極多比較（只以多模式組合為例）：

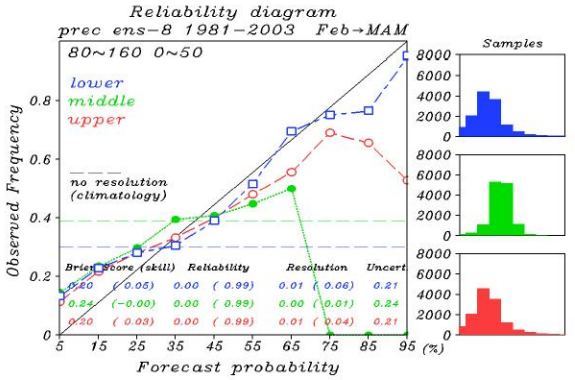

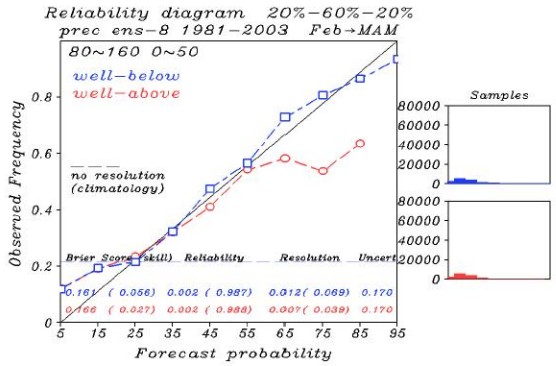

以五月起始，預報夏季（JJA）降雨距平的偏多與極多比較（只以多模式組合為例）：

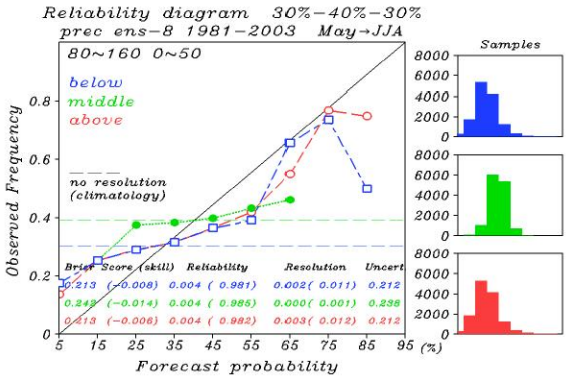

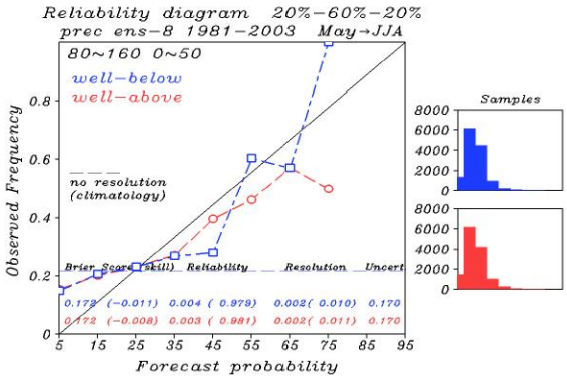

以八月起始，預報秋季（SON）降雨距平的偏多與極多比較（只以多模式組合為例）：

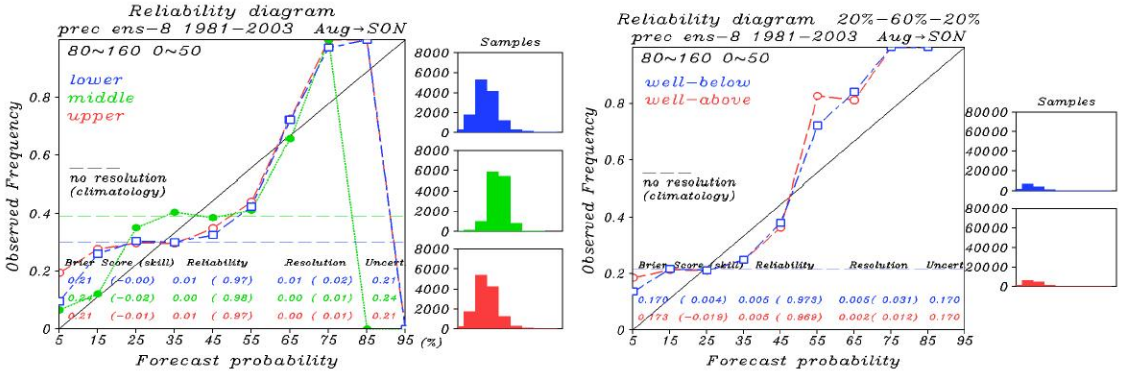

個別模式與多模式組合在預報極多的機率預報所得的Reliability Diagram 分布與 Brier skill score，與傳統三分類偏多時相似。

三、季節降雨預報的潛在經濟效益評估

計畫所建構的月季降雨預報系統的潛在經濟效益與應用價值分析，是年度計畫的另一個重點，儘管現階段沒有辦法直接與需要氣候資料的應用模式相結合，使用準備代價與損失的比值（cost/loss ratio）還是可以進行一些理想化的基礎分析。

3.1 在不同 cost/loss 比值所呈現的 Value Score 分布

根據之前的結果報告中得知，領先時間（lead time）越短模擬結果越佳，同樣的結果也顯現在economic value score中（參見計畫圖庫相關資料），故以下的討論先只針對初始的領先時間為主。若單純以cost/loss的比率變化來看，在「少雨」（below normal）的條件下，由圖 3.1 至圖 3.4 多重

超系集模式(ens-8)在四個不同月份中皆顯示當比率為0.3的時候能得到最佳的economic value score分布，隨著比率越大得到的分數分布越差，而若針對「多雨」(above normal)的情況分析，亦得到相同的結果(參見計畫圖庫相關資料)。計畫所建構的月季降雨預報系統的價值得分(Value score)，在東亞區域平均而言以 Cost/Lost=0.3 時最大，後續報告中的例子也以其為價值得分分布的主要呈現結果,最後的曲線圖則是檢視整個區域(或選擇區域)平均隨 Cost/Lost 比值的變化情形。

3.2 Value Distribution at Cost/Lost=0.3

將cost/loss的比率固定為0.3來分析，將各個單一模式與多模式組合(ens-8)相比較，在「多雨」的條件下，2月有明顯的大值分布一路從孟加拉灣延伸至菲律賓海上，依照模式的不同甚至有超過0.9以上接近perfect forecast的分數(圖 3.5)；5月各單一模式與ens-8結果不盡相同(圖 3.7)；8月以gfs-opgll_sh差異最大，echam4與ens-8的結果最為相近(圖 3.9)；11月多數單一模式表現出和ens-8相似的vs分布，除了ec5-opgll_sh、gfs-opgll_sh以外(圖 3.11)。改以「少雨」的條件來看，圖 3.6 的 2 月分布顯示ccm3和ncepgsm的表現最差；5 月的單一模式中仍舊是ccm3與ens-8差異最大(圖 3.8)；8月最佳分布為ens-8，相比之下差異最大的則為gfs-opgll_sh(圖3.10)；而圖3.12 顯示11月不論在單一模式或ens-8所得的分布相當近似，與ens-8相比之下單一模式當中ec5-opgll_sh有明顯低估的情形(圖3.12)。以vs的東亞分布來說不論是在「多雨」或「少雨」的條件下2月和11月看起來具有較為明顯的結果分布。

個別模式與多模式組合在value score為正的區域相仿，東亞區域尤其在較高緯度，月季降雨距平預報即使在Cost/lost=0.3 時，此預報系統並無法

呈現應用方面的價值。

3.3 Value Curve

由東亞地區取三個不同大小的範圍（分別為Large：80~160E，0~50N；Middle：100~140E，12.5~37.5N；Small：110~130E，20~30N）經過區域平均後得到的value score表現在圖 3.13 到 3.16 的曲線圖中。圖中即便不同模式、不同月份、不同領先時間、不同的區域所呈現的曲線都顯示一個最大的Value score 值落在cost/loss ratio等於0.3之處。先以多雨的情況來看，圖 3.13 的模式當中ccm3、gfs-cfs_sh和gfs-opg11_sh的區域平均結果最不理想，而雖然不同模式間最佳的曲線不盡相同，但大致說來2月比8月表現良好、lead-123比其他的領先時間表現良好、兩個範圍小的區域結果也遠勝東亞平均。而5月和11月明顯表現最差的是gfs-opg11_sh（圖 3.14），占多數的模式結果顯示11月的值高於5月，且多以lead-123為最佳。接著再看看少雨的情形，圖3.15顯示below normal在2月和8月沒有特別明顯的特徵，而圖 3.16 除了較差的gfs-opg11_sh和ncepgsm之外,11月的lead-123同樣有最佳的曲線。

將上述的vs值依照各項變數統計其機率密度以柱狀圖顯示在圖 3.17 和圖 3.18 中，總結來說，選取的區域範圍越小、領先時間越短潛在經濟價值得分的結果越佳；而四個季節當中又以11月表現最好，2月次之；多雨和少雨的條件對value score的影響差距不大；就模式而論，多模式組合(ens-8)比平均單一模式的表現較佳,如果想更細部探究不同單一模式之間與ens-8的分部差異可以參考圖3.18（上圖）。

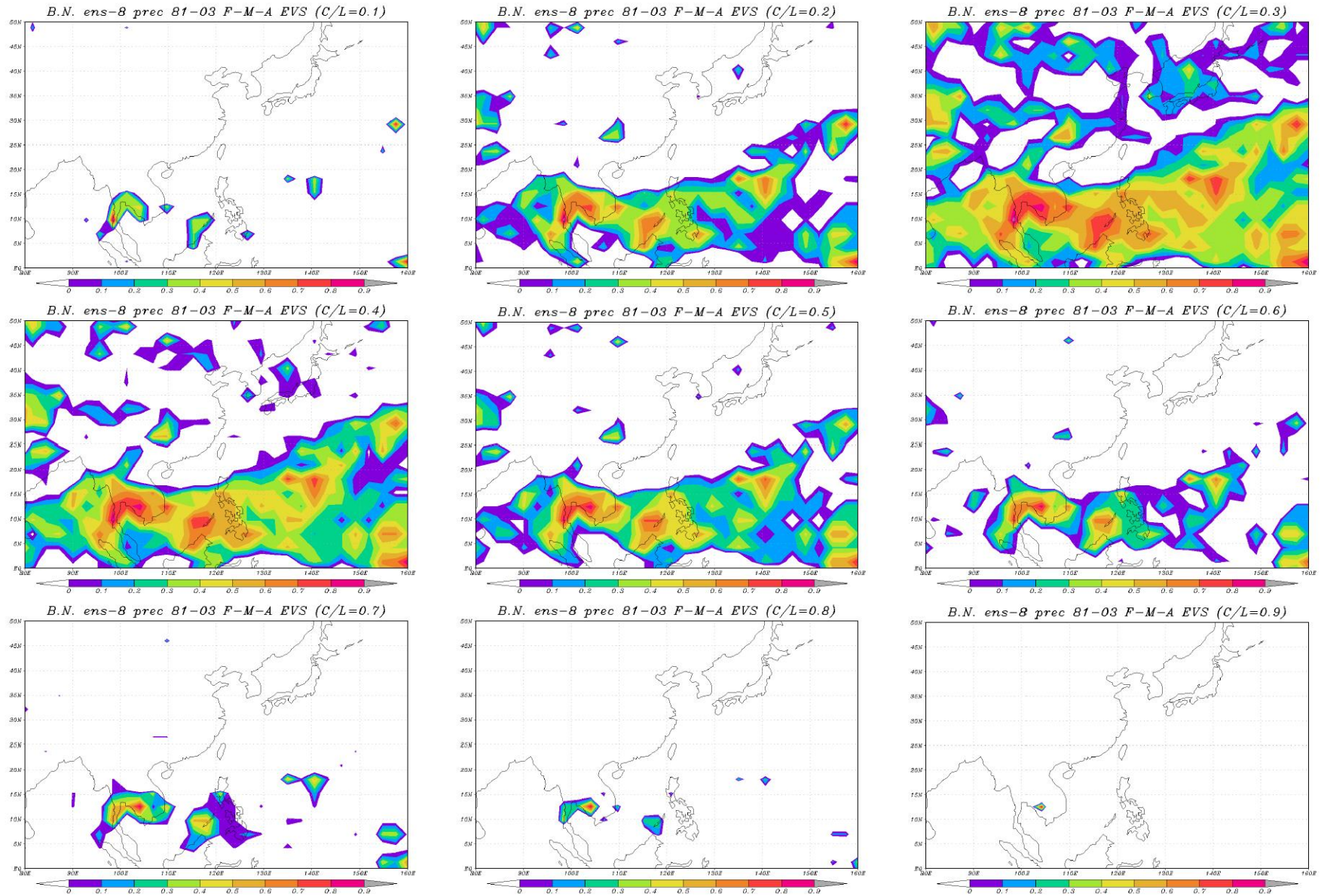

圖 3.1 、2 月 ens-8 在 below normal 下不同 cost/loss ratio 的 value score 分布

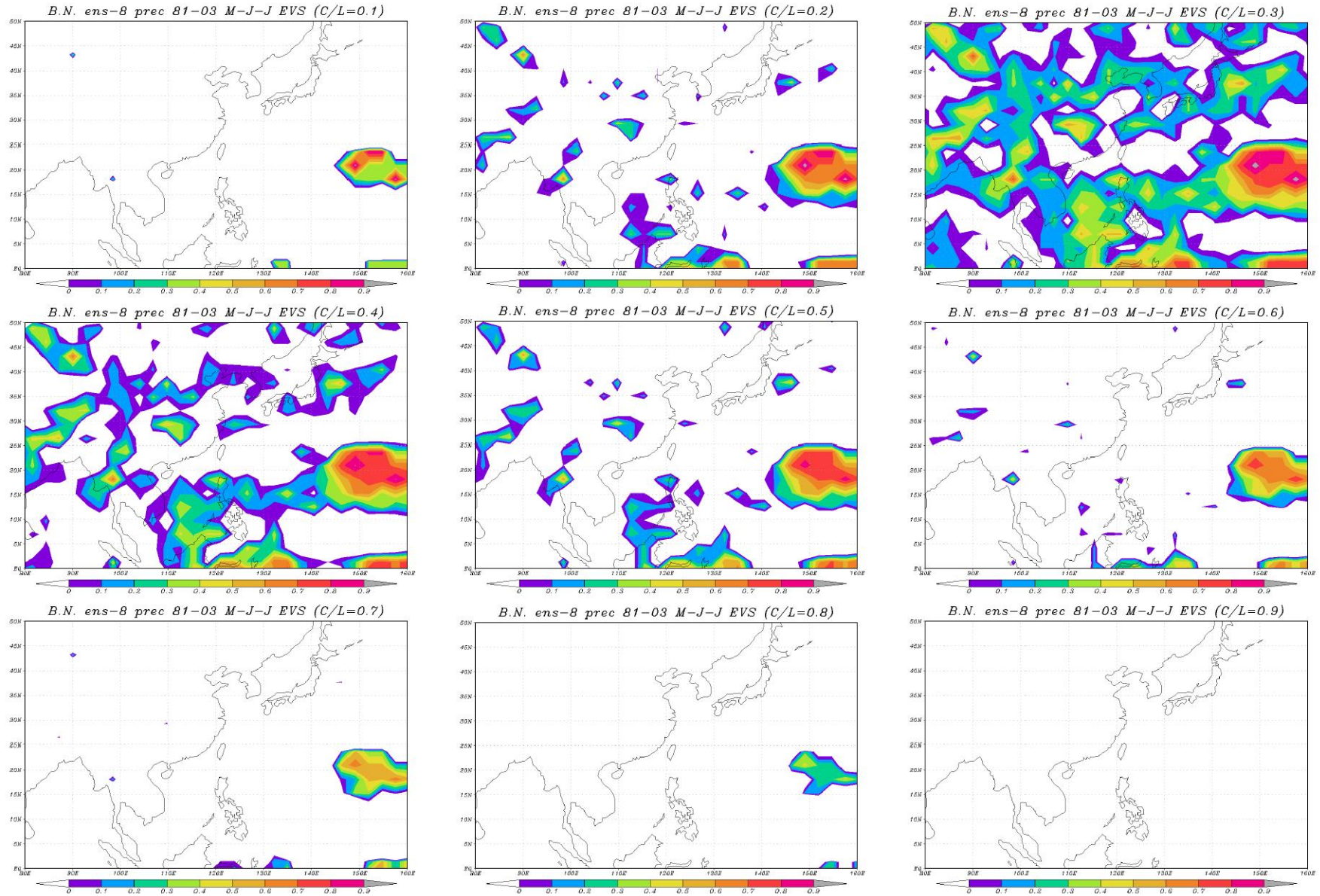

圖 3.2 、5 月 ens-8 在 below normal 下不同 cost/loss ratio 的 value score 分布

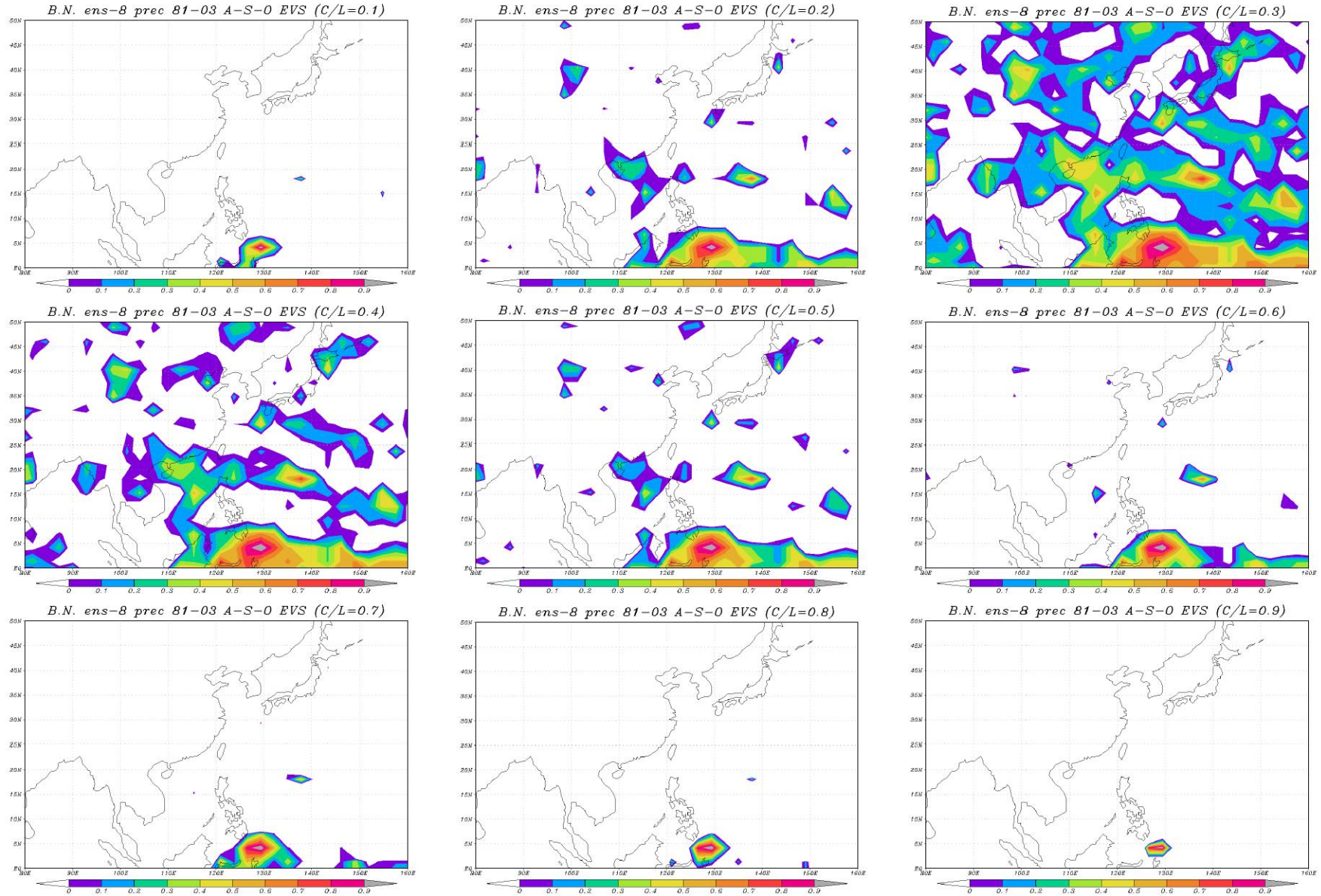

圖 3.3 、8 月 ens-8 在 below normal 下不同 cost/loss ratio 的 value score 分布

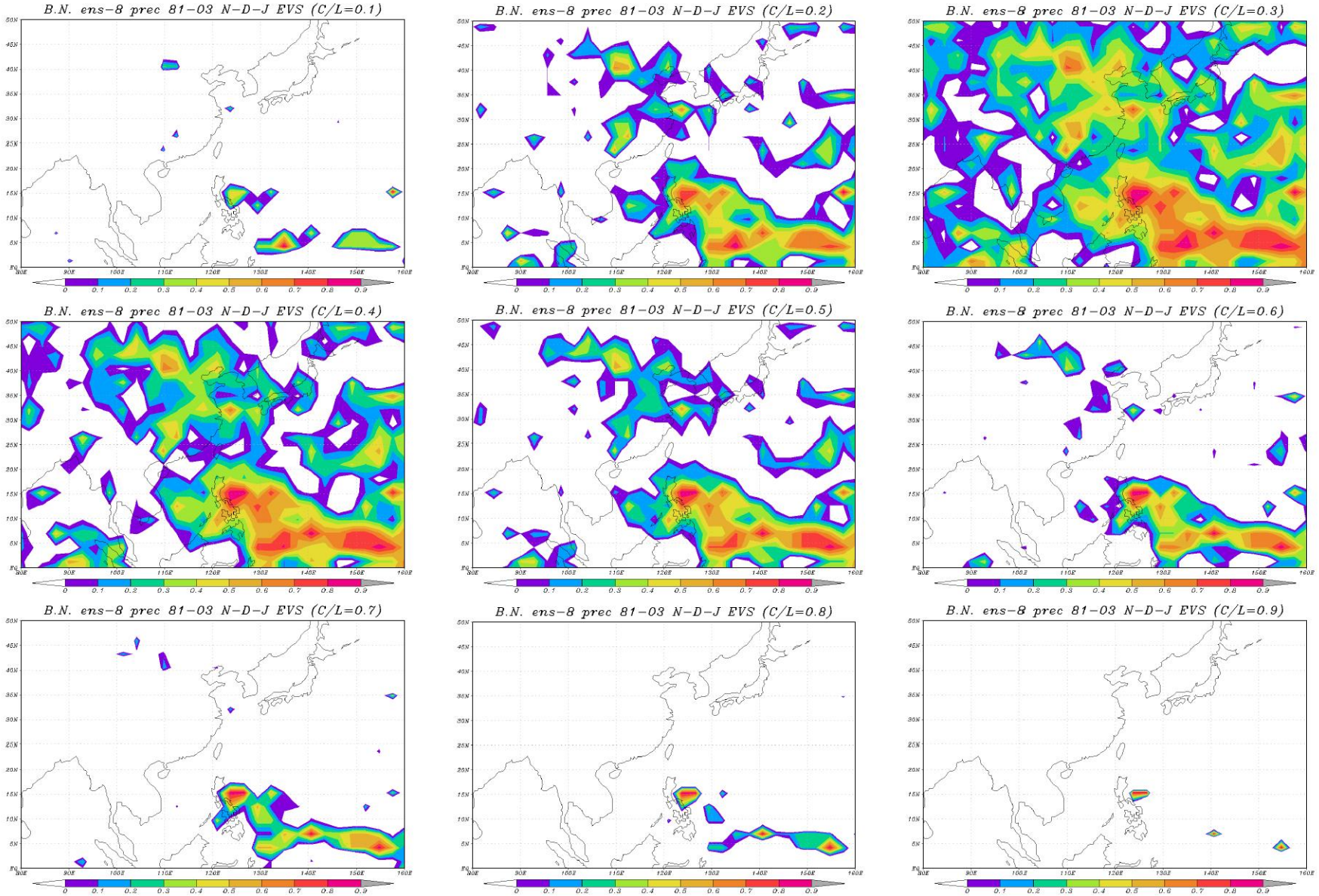

圖 3.4 、11 月 ens-8 在 below normal 下不同 cost/loss ratio 的 value score 分布

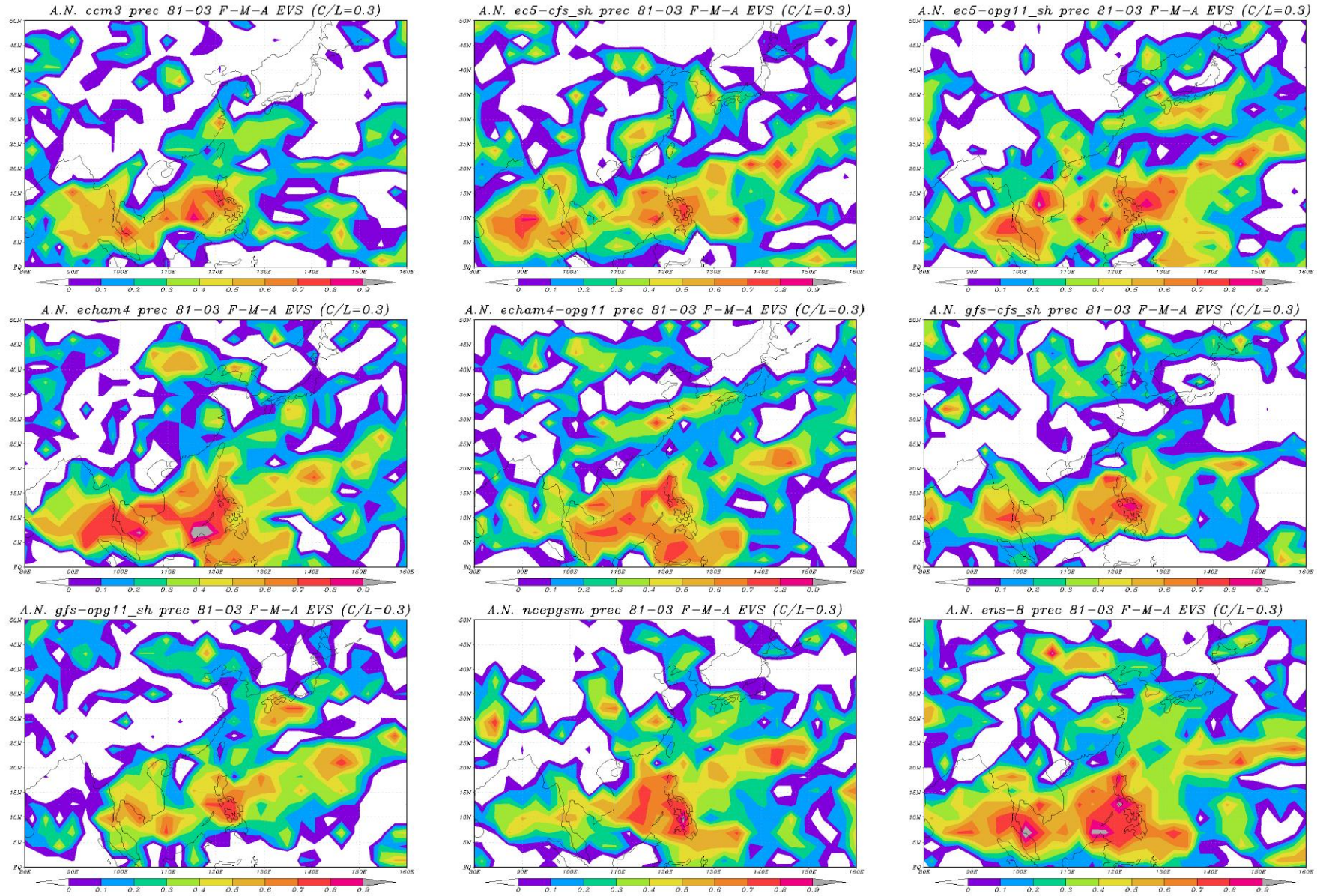

圖 3.5 、2 月 above normal 之 value score 東亞分布 (由左至右分別為 ccm3、ec5-cfs_sh、ec5-opg11_sh、echam4、echam4-opg11、gfs-cfs_sh、gfs-opg11_sh、ncepgsm、ens-8)

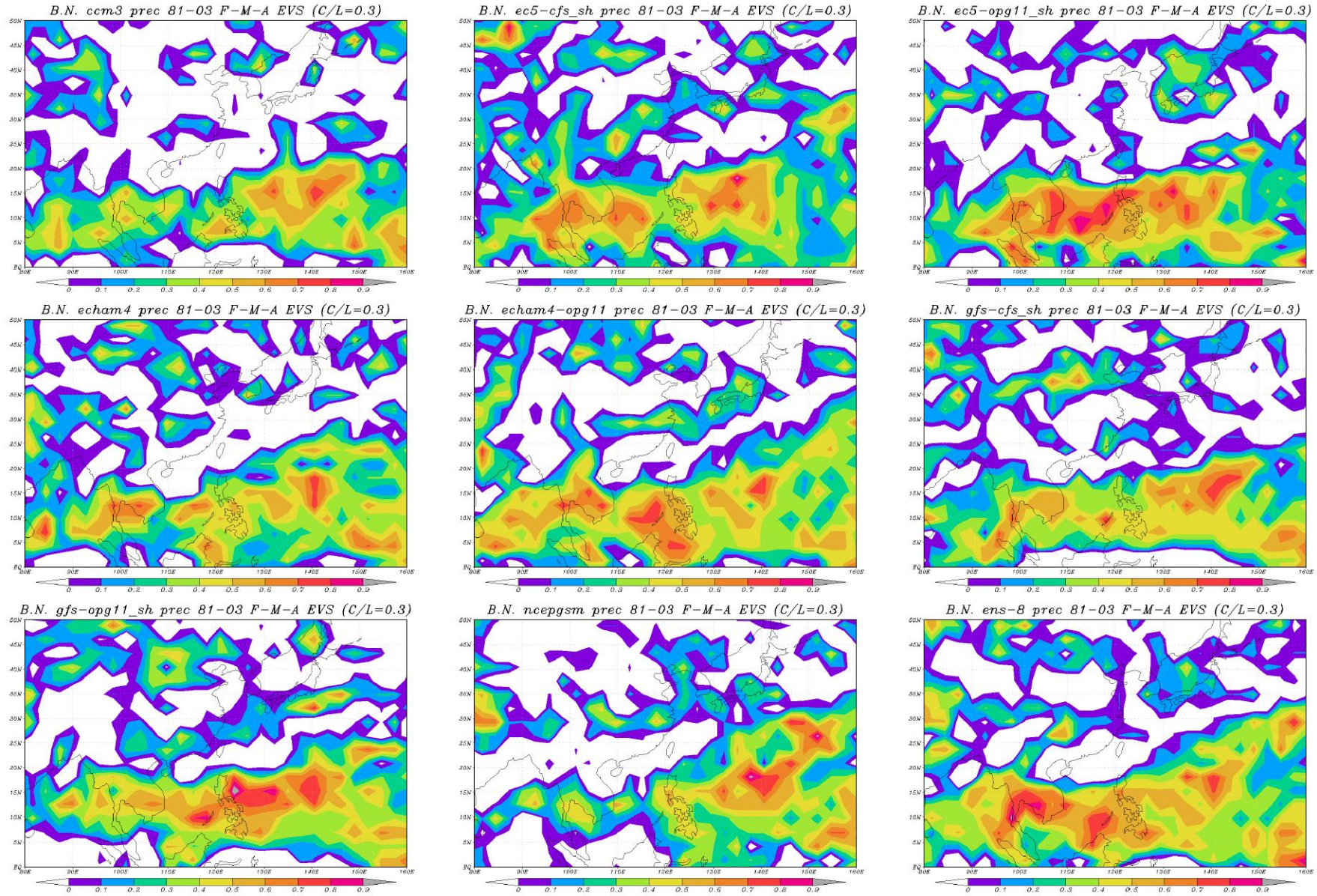

圖 3.6 、2 月 below normal 之 value score 東亞分布（由左至右分別為 ccm3、ec5-cfs_sh、ec5-opg11_sh、echam4、echam4-opg11、gfs-cfs_sh、gfs-opg11_sh、ncepgsm、ens-8)

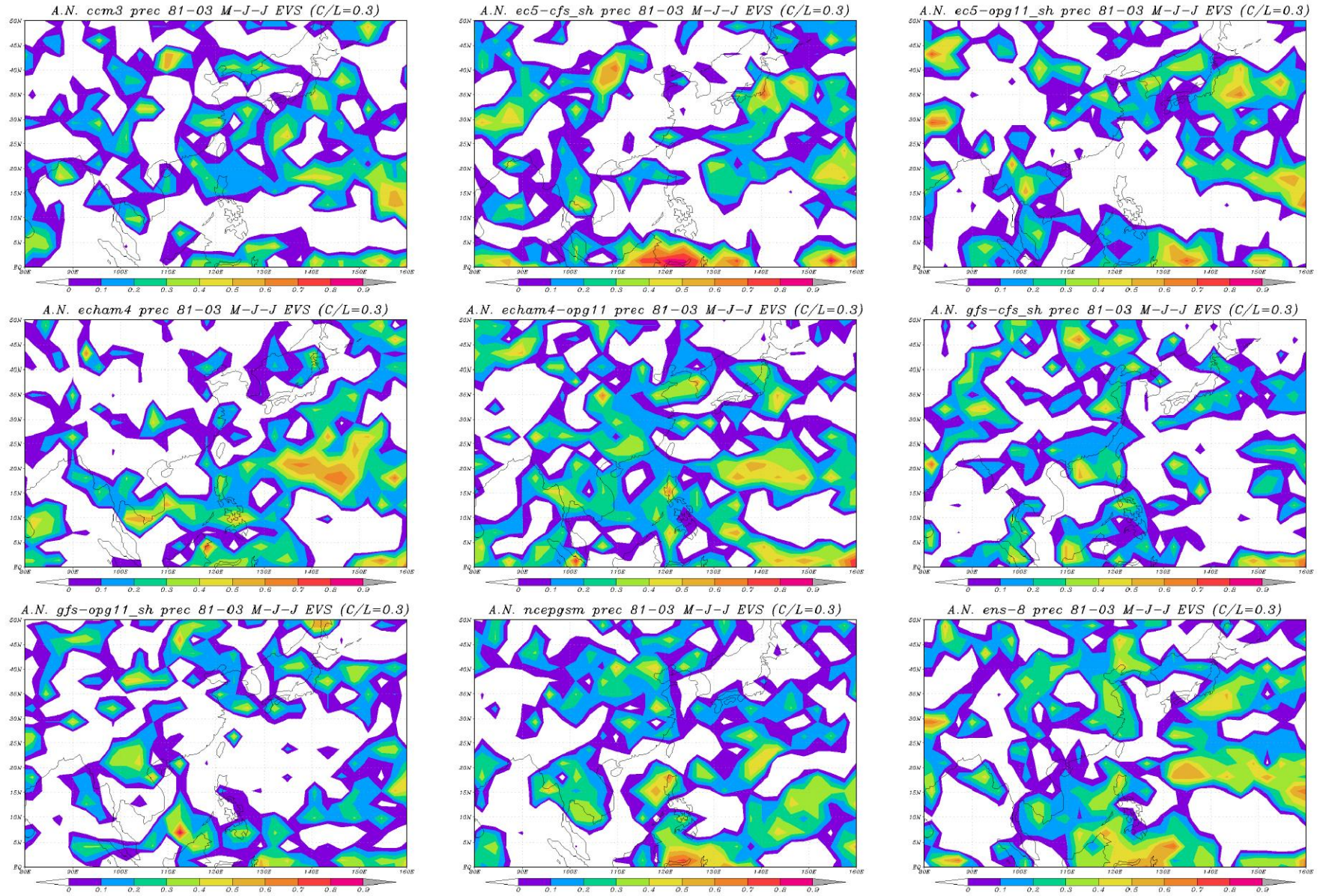

圖 3.7 、5 月 above normal 之 value score 東亞分布（由左至右分別為 ccm3、ec5-cfs_sh、ec5-opg11_sh、echam4、echam4-opg11、gfs-cfs_sh、gfs-opg11_sh、ncepgsm、ens-8)

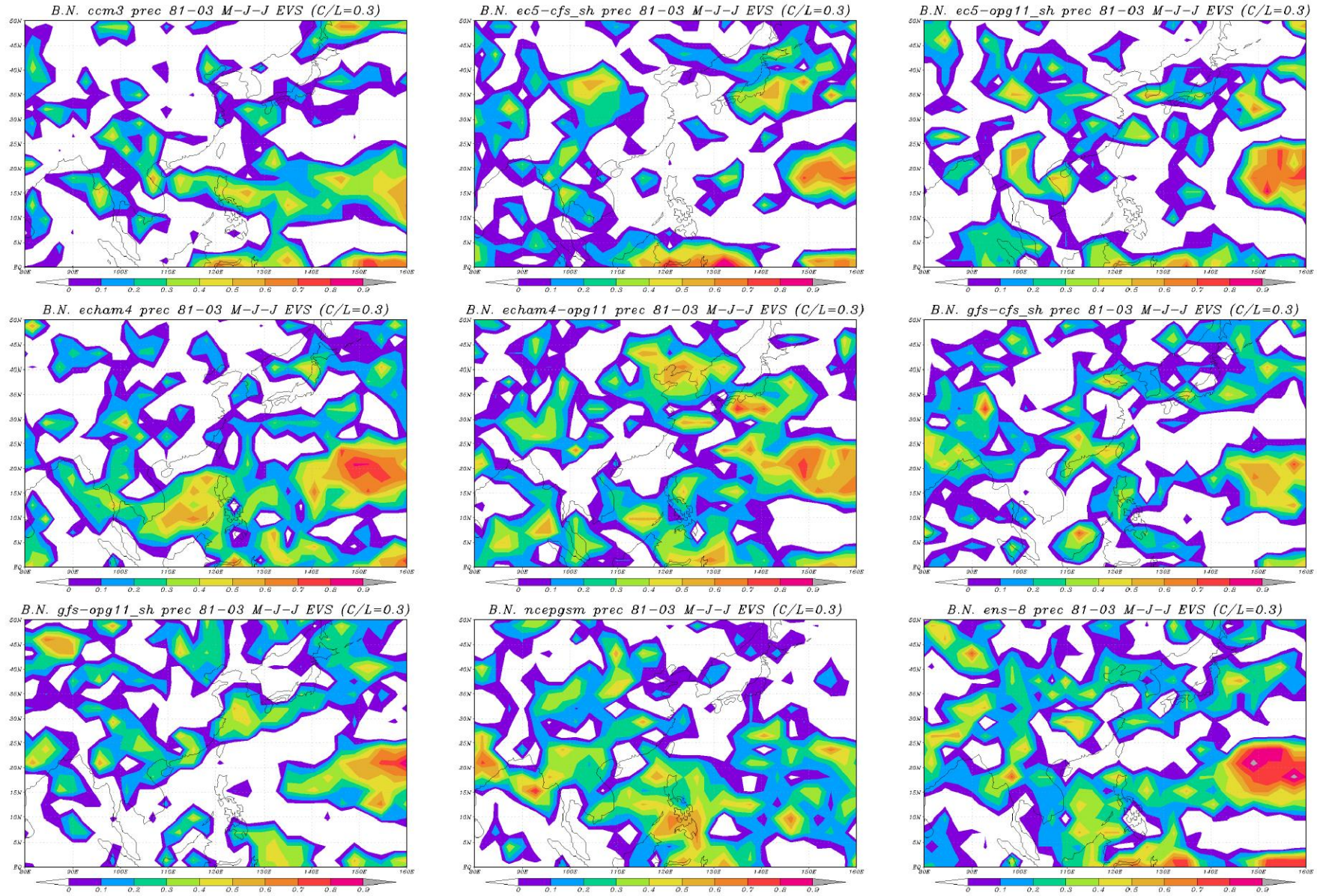

圖 3.8 、5 月 below normal 之 value score 東亞分布 (由左至右分別為 ccm3、ec5-cfs_sh、ec5-opg11_sh、echam4、echam4-opg11、gfs-cfs_sh、gfs-opg11_sh、ncepgsm、ens-8)

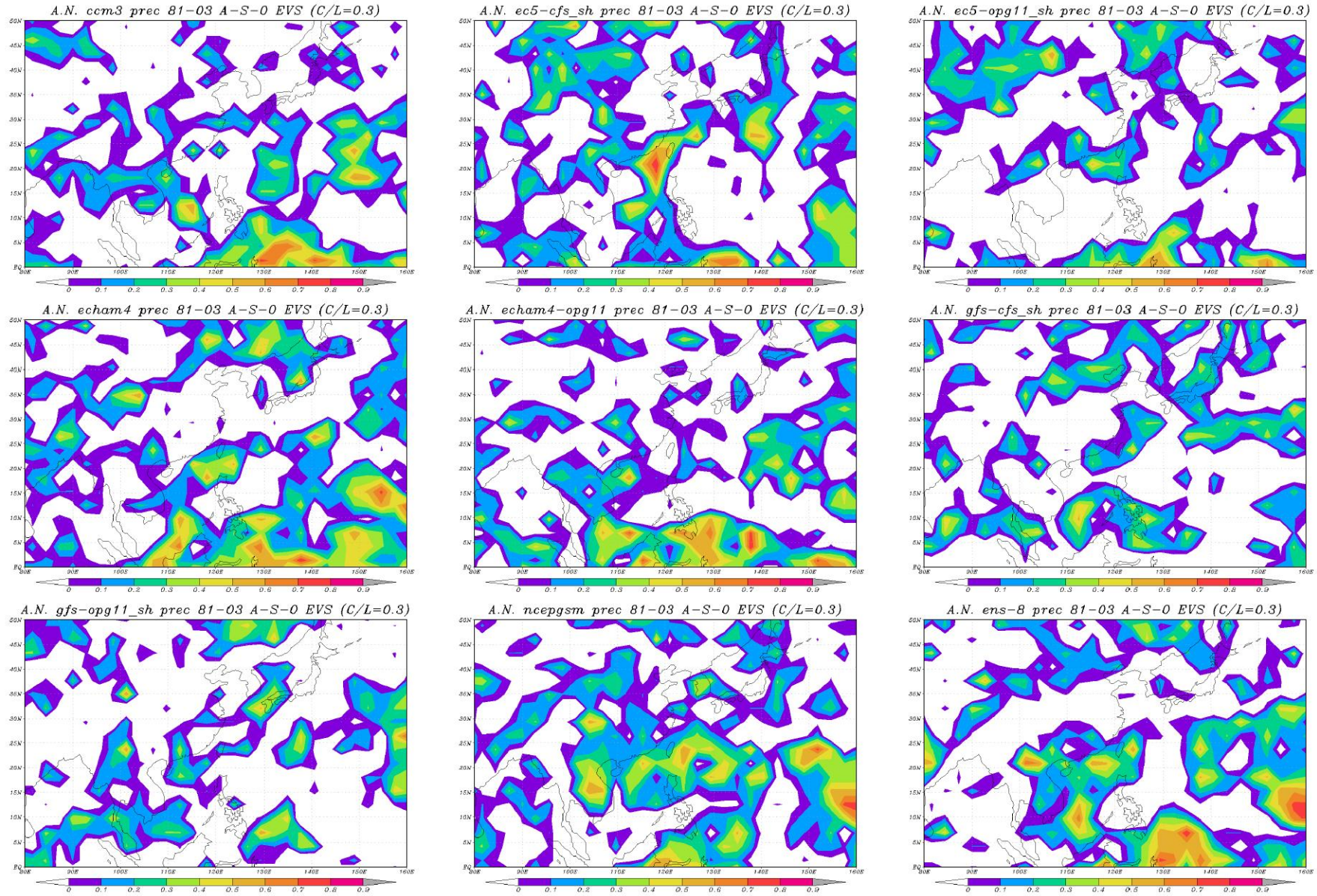

圖 3.9 、8 月 above normal 之 value score 東亞分布（由左至右分別為 ccm3、ec5-cfs_sh、ec5-opg11_sh、echam4、echam4-opg11、gfs-cfs_sh、gfs-opg11_sh、ncepgsm、ens-8)

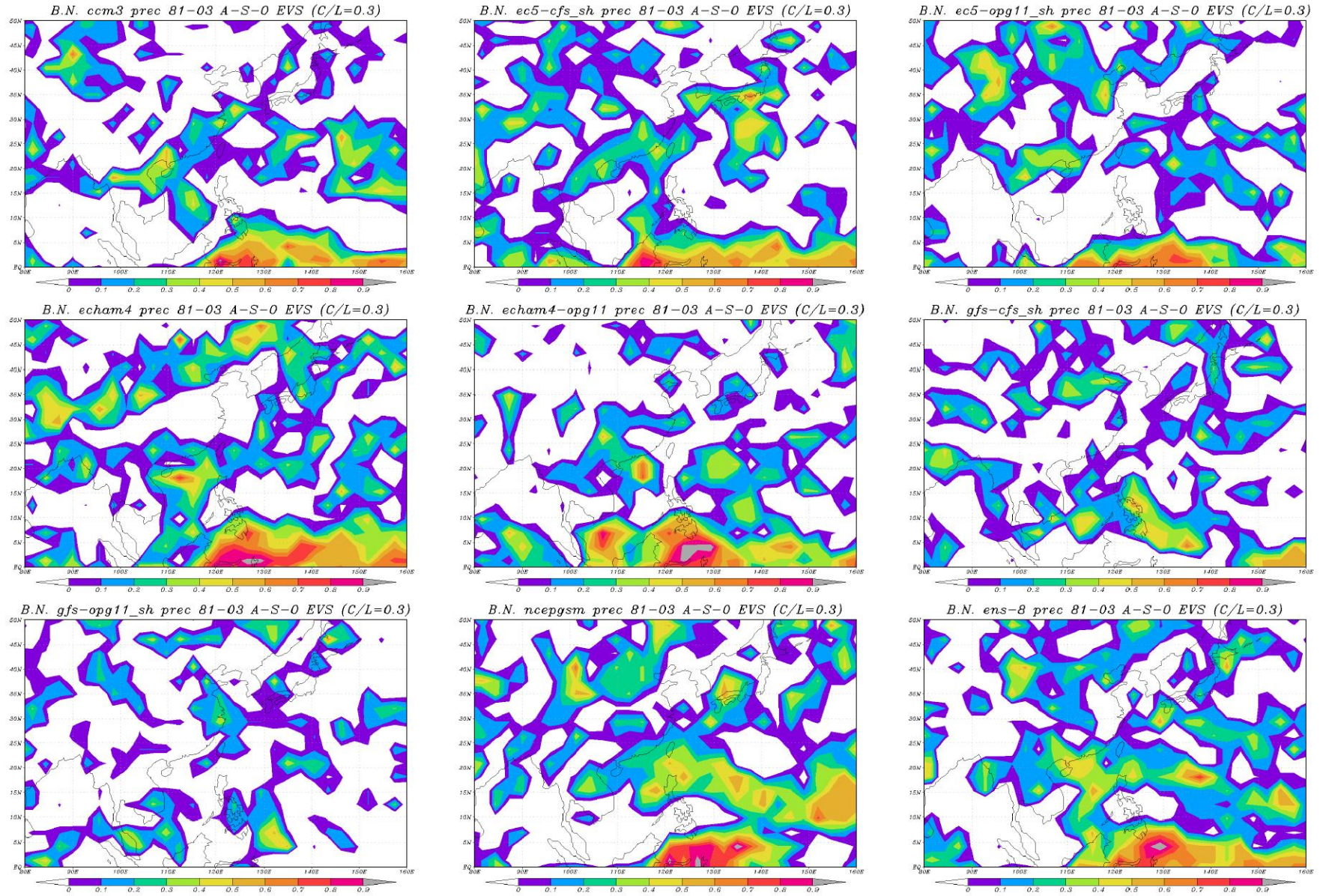

圖 3.10 、8 月 below normal 之 value score 東亞分布 (由左至右分別為 ccm3、ec5-cfs_sh、ec5-opg11_sh、echam4、echam4-opg11、gfs-cfs_sh、gfs-opg11_sh、ncepgsm、ens-8)

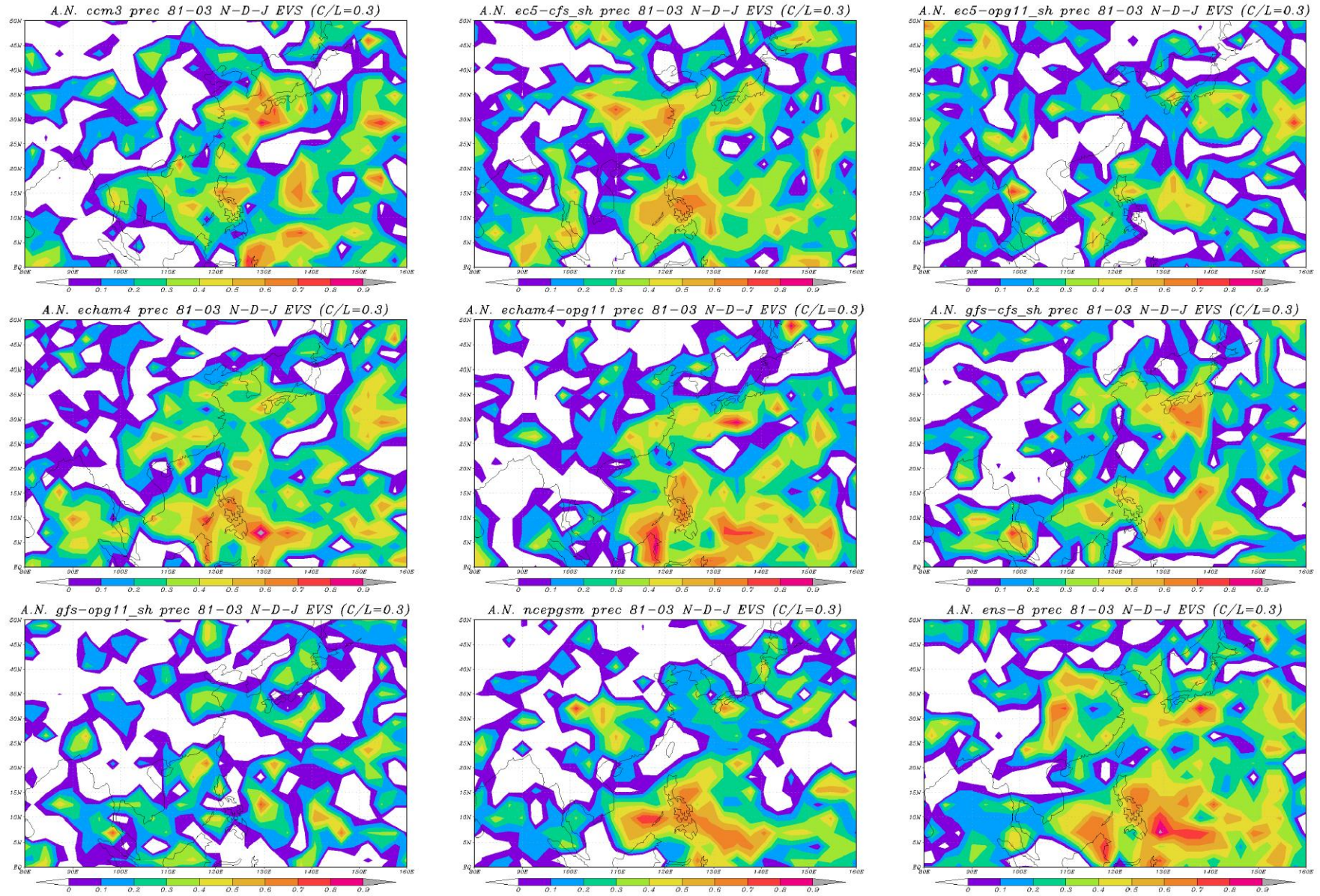

圖 3.11、11 月 above normal 之 value score 東亞分布 (由左至右分別為 ccm3、ec5-cfs_sh、ec5-opg11_sh、echam4、echam4-opg11、gfs-cfs_sh、gfs-opg11_sh、ncepgsm、ens-8

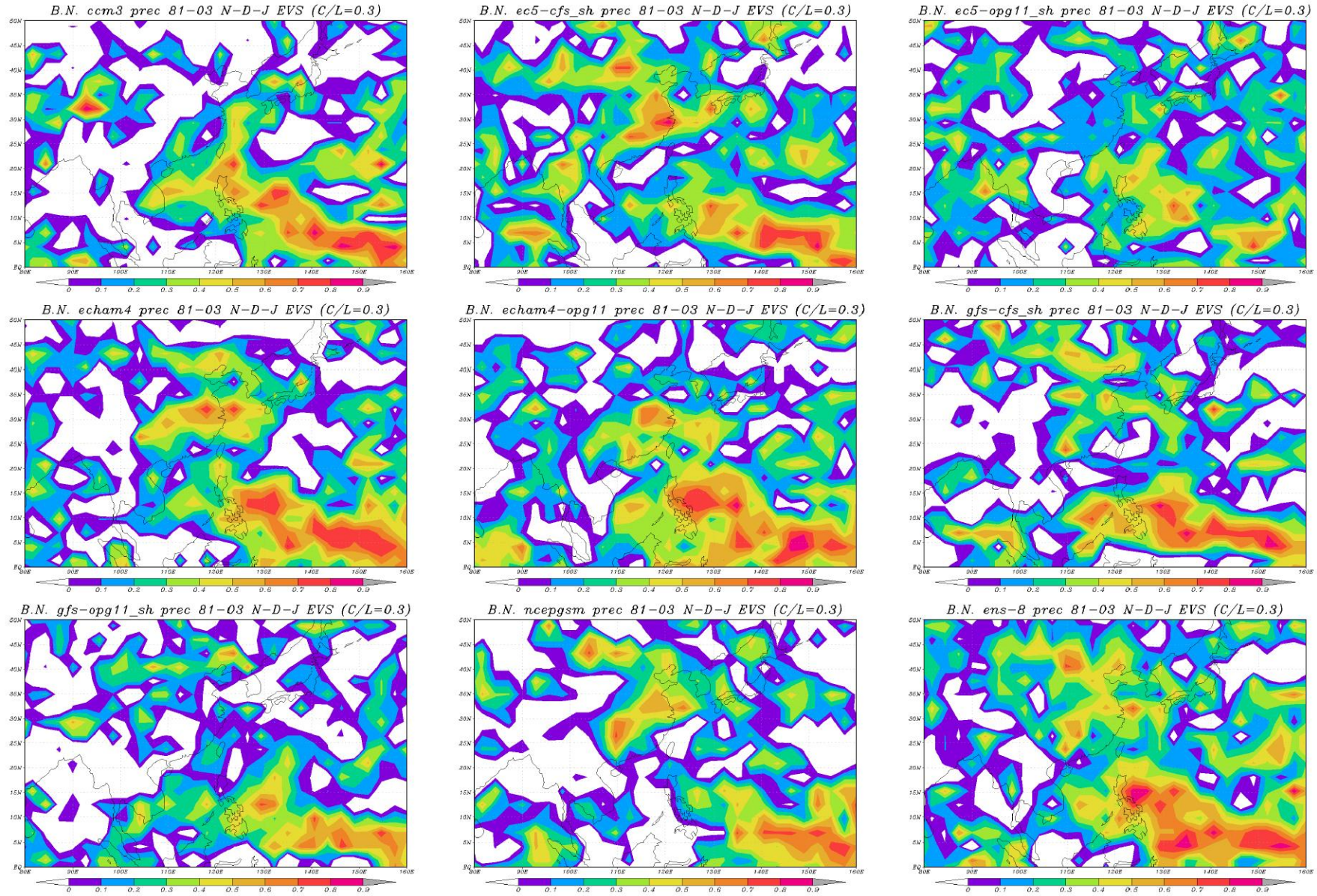

圖 3.12 、11 月 below normal 之 value score 東亞分布 (由左至右分別為 ccm3、ec5-cfs_sh、ec5-opg11_sh、echam4、echam4-opg11、gfs-cfs_sh、gfs-opg11_sh、ncepgsm、ens-8)

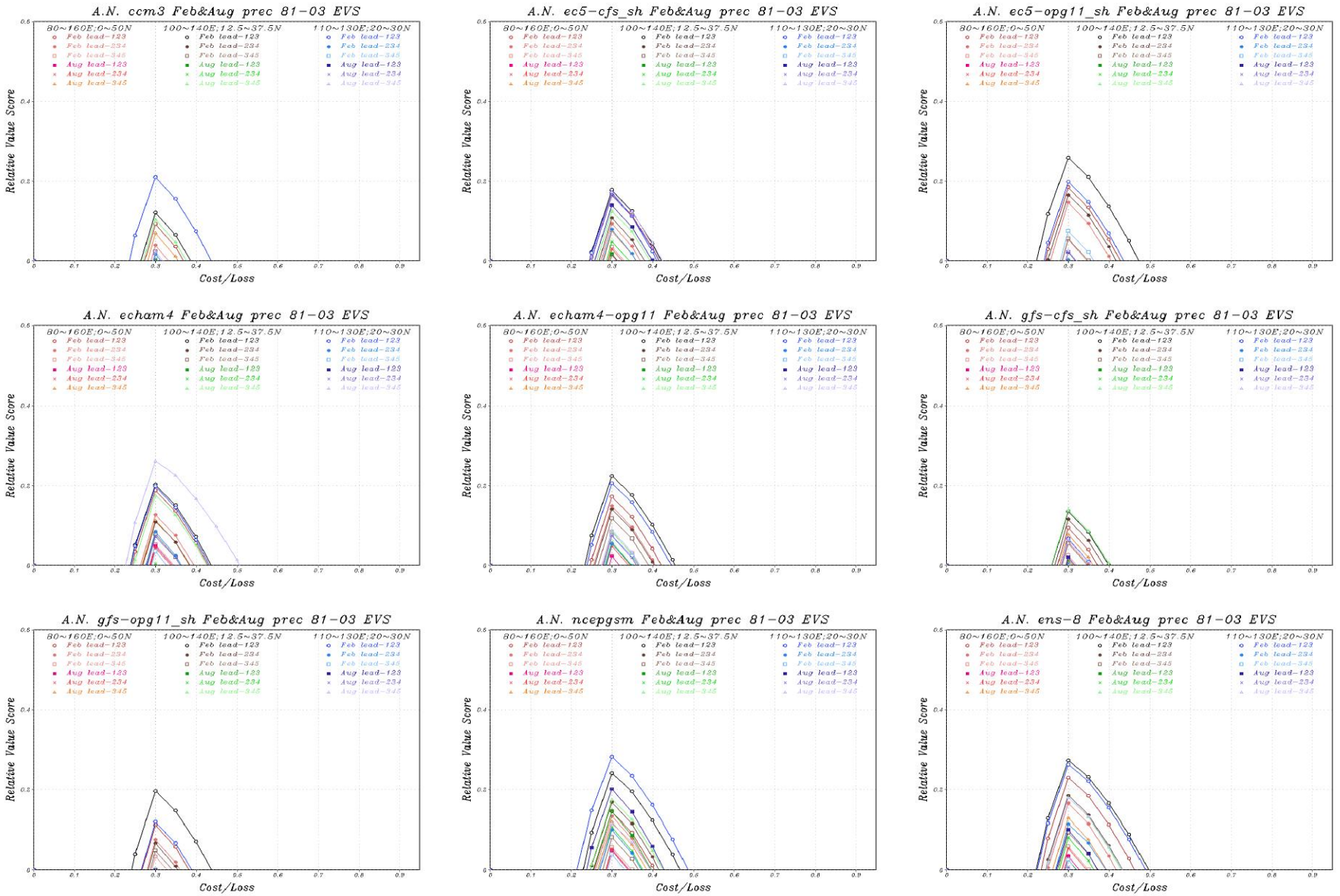

圖 3.13 、3 個不同東亞地區 domain 2 月和 8 月 above normal 之 value score curve(由左至右分別為 ccm3、ec5-cfs_sh、ec5-opg11_sh、echam4、echam4-opg11、gfs-cfs_sh、gfs-opg11_sh、ncepgsm、ens-8)

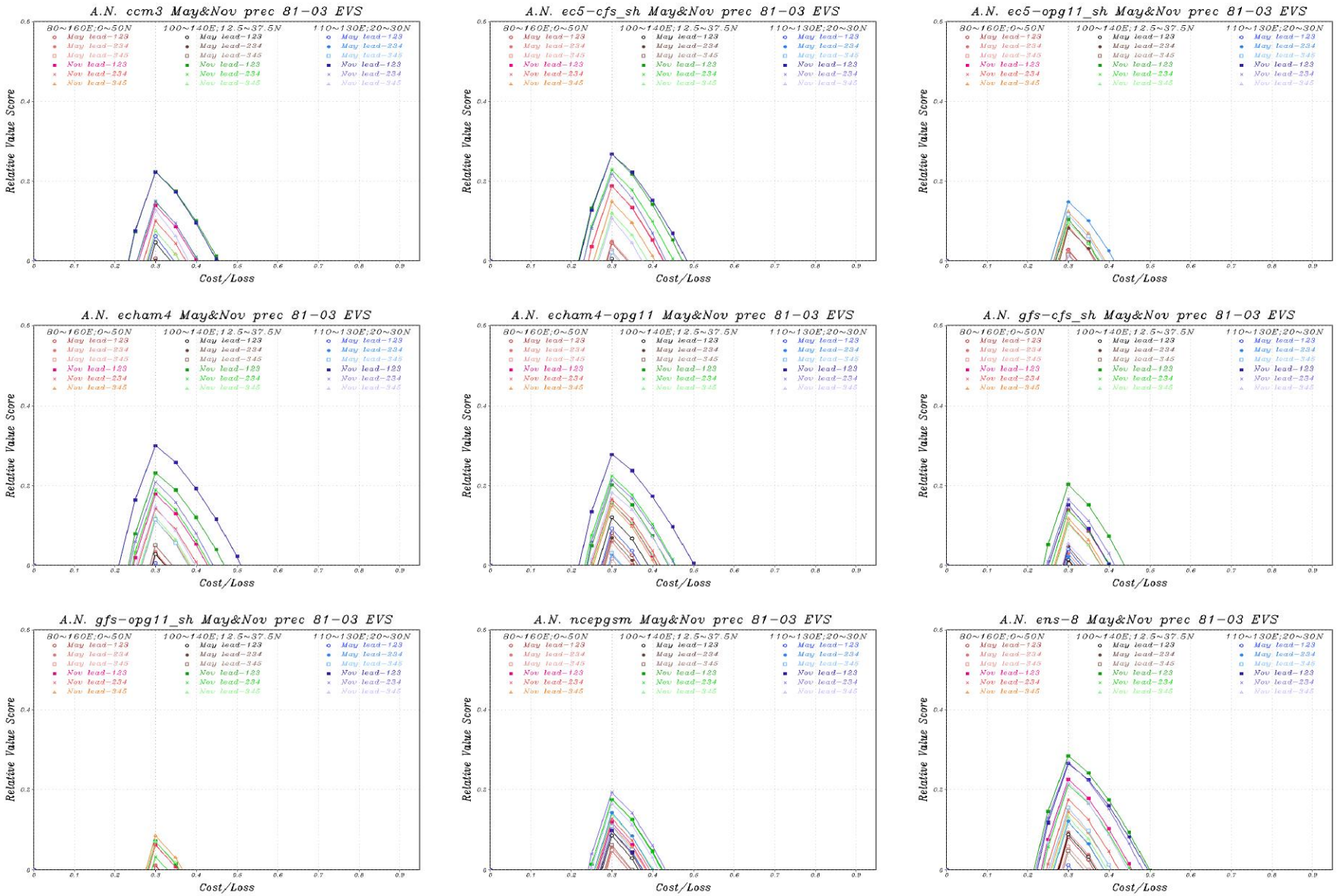

圖 3.14 、3 個不同東亞地區 domain 5 月和 11 月 above normal 之 value score curve(由左至右分別為 ccm3、ec5-cfs_sh、ec5-opg11_sh、echam4、echam4-opg11、gfs-cfs_sh、gfs-opg11_sh、ncepgsm、ens-8)

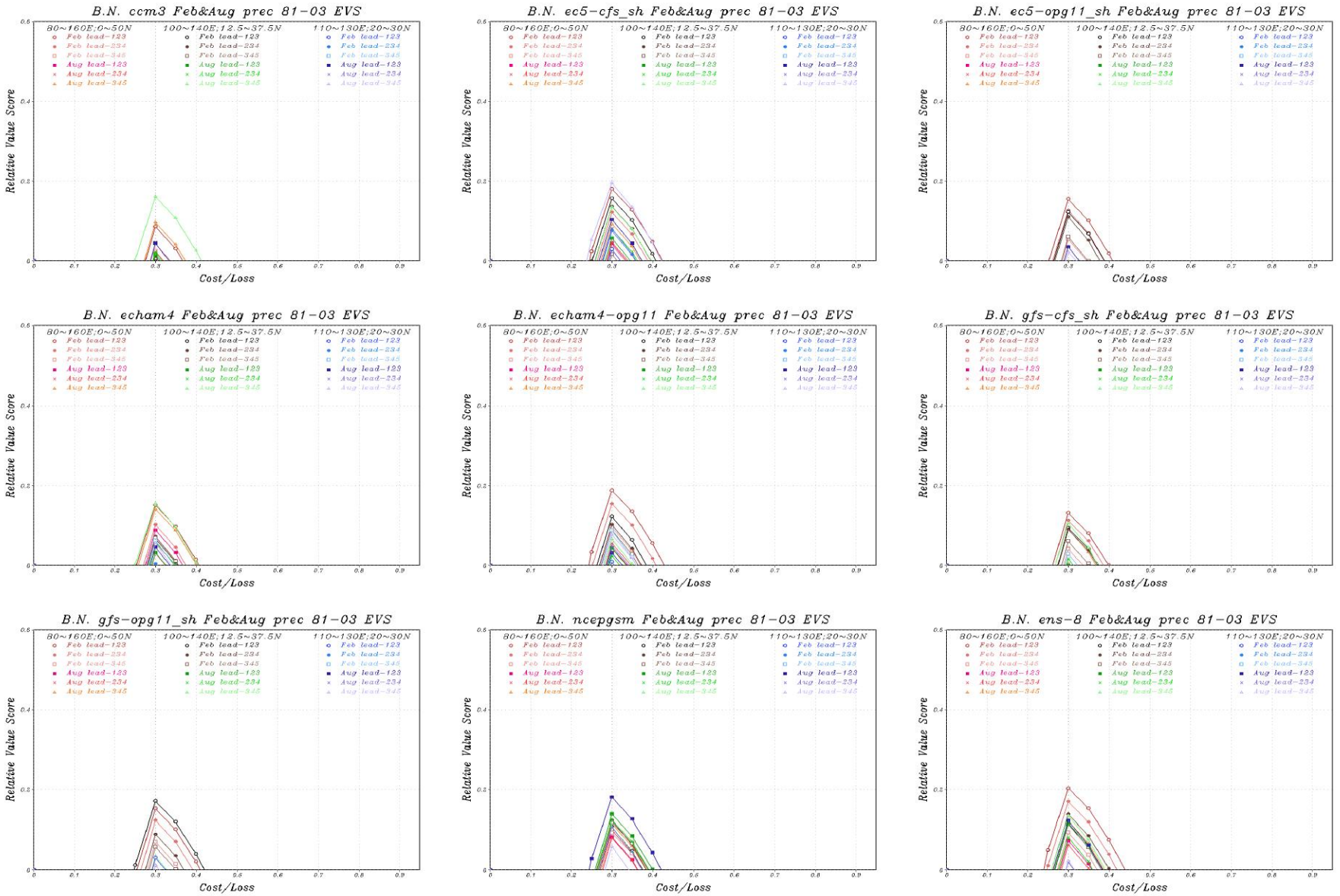

圖 3.15 、3 個不同東亞地區 domain 2 月和 8 月 below normal 之 value score curve(由左至右分別為 ccm3、ec5-cfs_sh、ec5-opg11_sh、echam4、echam4-opg11、gfs-cfs_sh、gfs-opg11_sh、ncepgsm、ens-8)

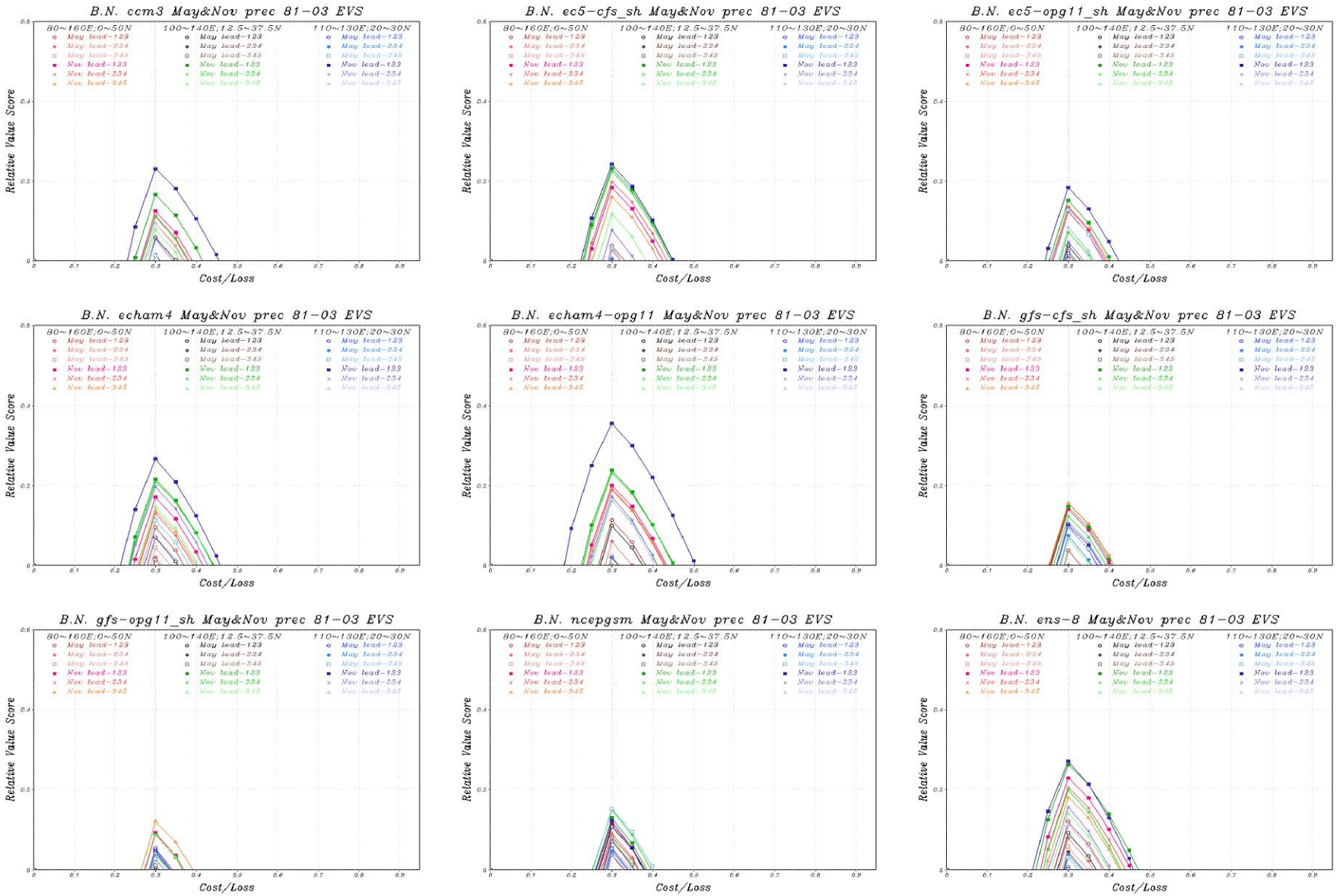

圖 3.16、3 個不同東亞地區 domain 5 月和 11 月 below normal 之 value score curve(由左至右分別為 ccm3、ec5-cfs_sh、ec5-opg11_sh、echam4、echam4-opg11、gfs-cfs_sh、gfs-opg11_sh、ncepgsm、ens-8)

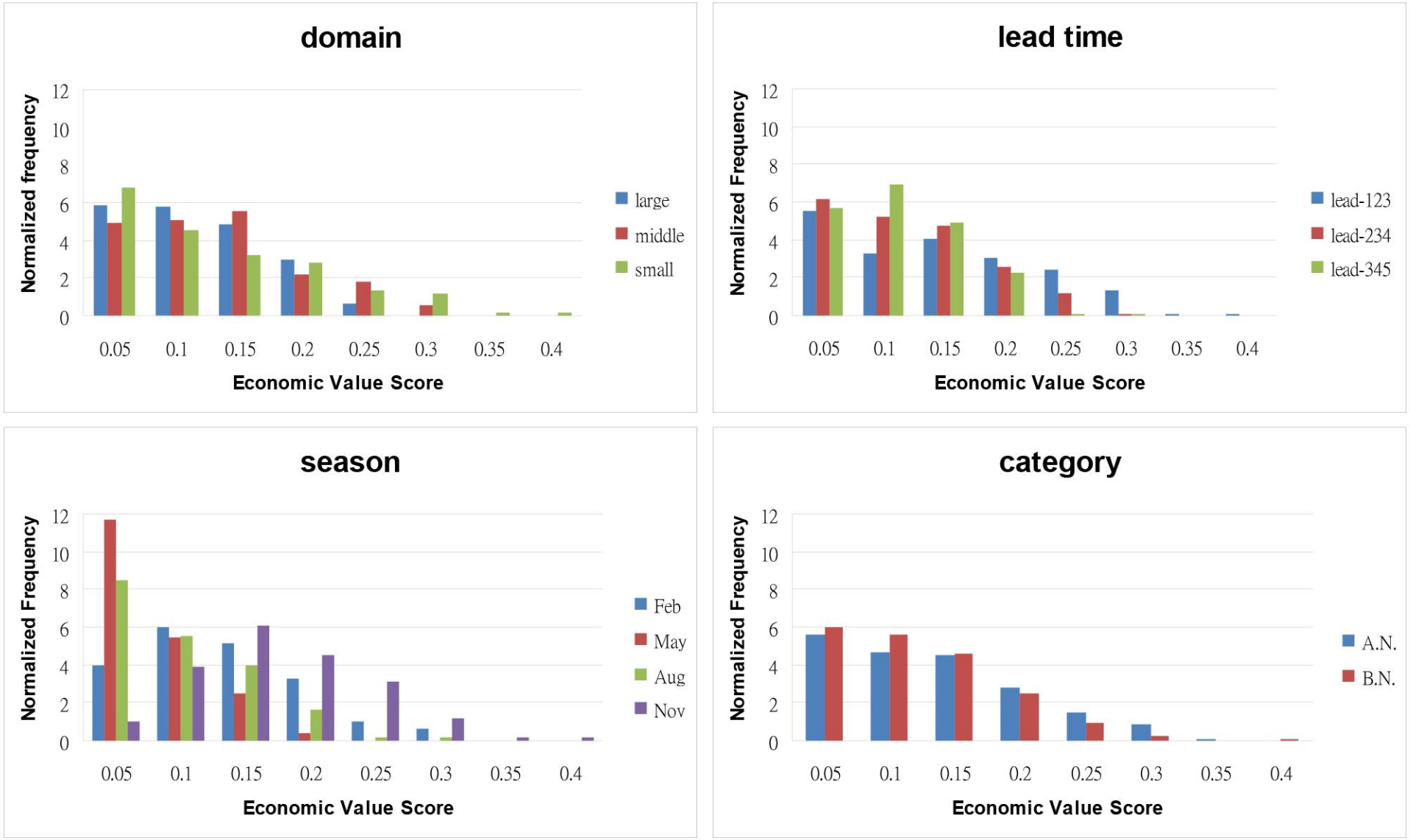

圖 3.17、統計各項變數之機率密度函數圖

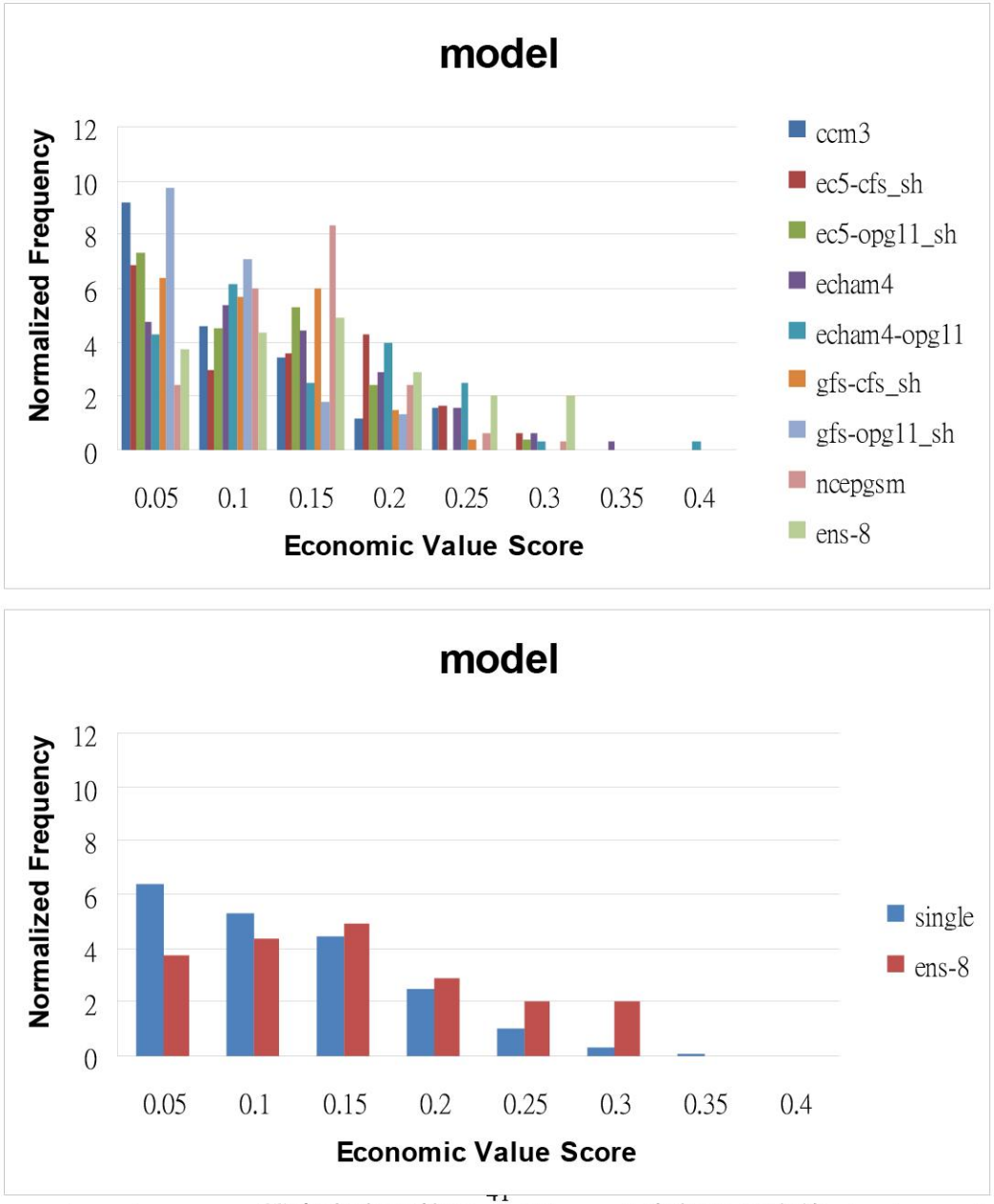

圖 3.18、(上)依不同模式的 Economic value score 機率密度函數圖；(下)ens-8 與經過平均的 single model 之機率密度函數圖

Seasonal Forecast for Local Precipitation over northern Taiwan using Statistical Downscaling

Jung-Lien Chu*[1], Hongwen Kang[2], Chi-Yung Tam[2], Chung-Kyu Park[2,3] and Cheng-Ta Chen[1]

[1]Department of Earth Sciences, National Taiwan Normal University, Taipei, Taiwan

[2]APEC Climate Center (APCC), Busan, Republic of Korea

[3]Korea Meteorological Administration, Seoul, Republic of Korea

Submitted to J. of Geophysical Research

Manuscript

September 28, 2007

Corresponding author address:
Jung-Lien Chu
Department of Earth Sciences, National Taiwan Normal University, No.88, Sec. 4, Tingzhou Rd., Wenshan District, Taipei 116, Taiwan.
Tel. +886-2-2930-9545 ; Fax. +886-2-2930-9545
E-mail: jlchu@rain.geos.ntnu.edu.tw

Abstract

This study investigates the potential of predicting local precipitation over northern Taiwan using statistical downscaling of large-scale circulation variables from global climate models (GCMs). Historical hindcast data of 500 hPa geopotential height (Z500) and sea level pressure (SLP) from six different GCMs, with the target season of being that of June, July, and August (JJA), are used as ?predictors for downscaling. Singular value decomposition analysis (SVDA) using observational data reveals that the rainfall over northern Taiwan is strongly coupled with a prominent tripole pattern of Z500 (SLP) field over the western North Pacific/East Asian coast. SVDA using model SLP or height field and station rainfall as input also gives similar results, indicating that most models can capture this mode of co-variability. SLP and Z500 from models are then used for local rainfall prediction based on their relationship, which is drawn from the SVDA. For every station considered in this study, downscaled prediction shows considerable improvement when compared with model output. In particular, downscaling is able to correct the erroneous sign of model rainfall prediction. However, a few models show very low skill in their downscaled precipitation. For these models, the correlation between observed rainfall and simulated Z500 (SLP) leading SVD patterns is found to be weak. The performance based on the average of downscaled prediction using Z500 and SLP is also evaluated. In general, the average prediction is more stable and skillful when compared with results based on one predictor. Overall, this study demonstrates that useful regional climate information can be obtained from downscaling using large-scale variables from coarse-resolution GCM products.

1. Introduction

The East Asian Summer Monsoon (EASM) region is noted for its complex space-time rainfall variability. The complexity of the monsoon system makes it hard to have skillful predictions in the EASM region. General circulation models (GCMs) have become the main tool for seasonal prediction. Though large-scale features of atmospheric variability in the tropics can be reasonably captured (see, e.g., Lau 1985; Rowell 1998), GCMs still have considerable difficulties in faithfully simulating regional climate correlations (Gortch and MacCracken 1991; Xu 1999). Owing to their relatively coarse resolution, land-sea contrast and topography in the regional scale cannot be properly represented in global models. The difficulty in skillfully predicting the EASM broad-scale climate using GCMs makes regional climate forecast an even more challenging problem (Sperber and Palmer 1996; Wang et al. 1998; Sperber et al. 2001; Kang et al. 2002).

Various methods of downscaling have been developed in order to overcome the inadequacies of GCMs in simulating local climate conditions. They can be categorized into two types. One is the method of dynamical downscaling. High-resolution simulation is obtained using a regional climate model, which in turn is driven by the outputs of a coarser resolution GCM. This method has the potential of simulating extreme events (Diez et al. 2005). However, high-resolution simulations can be computationally expensive, and a lot of storage space is required for archiving model outputs. The other type is statistical downscaling (von Storch et al. 1993). The goal is to discover a stable relation between GCM outputs and a variable of the local climate. This relationship is exploited in order to predict elements of the regional climate using GCM products. Statistical downscaling has come to be widely used because of its lesser computational requirement.

Most statistical downscaling schemes are based on regression or similar methods (Giorgi et al. 2001, Benestad 2004). Wetterhall et al. (2005) used sea level pressure (SLP) as a predictor and found increased skill in predicting the seasonal mean precipitation using analogue-based downscaling. Feddersen and Andersen (2005) also reports skillful predictions of temperature and precipitation by statistical downscaling.

The focus of this study is the application of statistical downscaling for regional climate prediction over Taiwan. In particular, a downscaling scheme for predicting summer precipitation over northern Taiwan will be developed. The results of downscaling based on various GCM hindcast experiment datasets will be analyzed. The outline of this study runs as follows. Section 2 introduces the model data used and the method of downscaling. Analyses and results of downscaling are described in section 3. A summary and some discussions are presented in section 4.

2. Data and methodology

2.1. Model experiments and station data

In the present study, data from hindcast experiments from six different global models with the target season of June, July, and August (JJA) are used for statistical downscaling. These datasets are taken from the SMIP-type historical forecasts with one-month lead time, for the period of 1983-2003, SMIP being short for the Seasonal Prediction Model Intercomparison Project. They were run by six operational centers, and are archived at the Asia-Pacific Economic Cooperation Climate Center (APCC). For the hindcast experiments run by the Central Weather Bureau (CWB), the Hydrometeorological Centre of Russia (HMC) and the Main Geophysical Observatory (MGO), the Sea Surface Temperature (SST) used in seasonal prediction is based on observed persistent SST anomalies. For the Japan Meteorological Agency (JMA) and

the Meteorological Research Institute (METRI), predicted SST information is used. The National Centers for Environmental Prediction (NCEP) forecasting system is a fully coupled model. Table 1 provides a summary of data sources and model experiments. All hindcast data are interpolated on a 2.5° x 2.5° grid for analyses.

Station data of precipitation over Taiwan for the period of 1950-2006 are provided by the CWB. Six of these stations in northern Taiwan are studied. Their locations are shown in Figure 1. In addition, NCEP-NCAR Reanalysis fields are also used as observational data in this study.

2.2 Choice of predictors

Statistical downscaling makes use of long-term GCM hindcast data to derive robust relationships between observations and model outputs. The information is then used for choosing suitable meteorological variables as predictors. Two conditions should be satisfied in selecting the right variable. One is that it has to be well simulated by the GCM (Wilby et al. 1999). The other is that there should be a stable relation between the predictor and the predictand. For instance, the variable with the highest correlation coefficient with the predictand can be a good choice for a predictor (Kang et al. 2007). Commonly-used large-scale variables for predicting precipitation include the geopotential height (von Storch 1999), SLP (Wetterhall et al. 2005), geostrophic wind (Wilby et al. 1998) and wind speed (Murphy 1999).

In addition to selecting predictors, it is also important to determine the domain over which predictor values are considered. The place where the correlation coefficient between a predictand and a predictor is zero can be considered to be the boundary of a domain (Benestad 2004). Another basis for the selection of a domain is that it should be large enough to resolve the relevant large-scale pattern and encompass corresponding observations (Feddersen et al. 2005).

Based on the results of correlation analyses between various large-scale variables and the station rainfall of interest, 500hPa geopotential height (Z500) and SLP are used as predictors and the domain of analysis is chosen to be 80°-160°E and 0°- 60°N.

2.3. Statistical downscaling method

In this study, a combination of EOF truncation and SVDA is used to obtain stable statistical relationships between large-scale circulation and regional precipitation. Before downscaling is applied, the time series of large-scale variables are reconstructed using their respective EOFs and principal components as a means of noise filtering. Here, the first ten leading modes for the large-scale variables are retained. SVDA is then used to extract coupled patterns between the two fields. A downscaling transfer function was constructed as follows:

$$PR_j(t,x) = \sum_{i=1}^{n} S_i(t) R_i(x)$$

Here $PR_j(t,x)$ indicates the downscaled prediction. $S_i(t)$ is the time expansion coefficient of the SVD mode for the large-scale predictor. $R_i(x)$ is the singular vector of the predictand, and n is the total number of SVD modes retained. Cross-validation was carried out to evaluate the skill of the downscaling scheme. The detail of the method of downscaling can be found in Kim et al. (2004), Feddersen et al. (1999), Feddersen et al. (2005), and Kang et al. (2004). The same process is repeated for the hindcast dataset of each of the six models. We also consider the results of downscaling obtained by averaging the six downscaled outputs from all models.

3. Results

3.1. Relationship between regional rainfall and observed large-scale circulation

For the purpose of obtaining a first glimpse of the inter-annual variability of

rainfall over northern Taiwan, an EOF analysis for JJA precipitation is carried out. The leading EOF pattern is given in Figure 2. This EOF mode accounts for 86% of the total variance, and is characterized by the same sign of rainfall anomalies at each station. As will be shown subsequently, this dominant mode is closely tied to the circulation over the EASM region.

SVD analysis is now used to unveil any robust modes of covariability between large-scale variables and station rainfall. Figure 3 gives spatial patterns for the first SVD mode using station precipitation and Z500 as input data, and those using precipitation and SLP. For the Z500 field, a tripole can be discerned in the East Asian region, which is characterized by a wave-like pattern with centers of action along the East Asian coast. There is a positive center over Taiwan, a negative center over Japan and the Korea peninsula, and a positive anomaly is found over the Sea of Okhotsk. The corresponding rainfall pattern shows suppressed precipitation for all stations over northern Taiwan, similar to the 1st EOF of rainfall (see Figure 1). A similar pair of patterns is found for the leading SVD mode for precipitation and SLP, with an obvious north-south oriented tripole corresponding to the latter precipitation field. The time series of expansion coefficients corresponding to the leading SVD mode for precipitation and Z500, and for SLP, are given in Figure 3c and 3f, respectively. The moderately high correlation between the expansion coefficients suggests that the rainfall and Z500 (or SLP) are coupled on interannual timescale. Overall, the results indicate that suppressed precipitation over northern Taiwan is associated with a large-scale tripole pattern in the SLP or Z500 field, with positive centers of action over Taiwan and also over the Sea of Okhotsk to northeastern Eurasia, and a negative center over Japan. In addition, the Squared Covariance Fraction (SCF) between Z500 (or SLP) and station precipitation for the first SVD mode is about 90%. These results

provide a basis for choosing Z500 and SLP in predicting station rainfall over northern Taiwan during JJA.

To further elucidate the relationship between the large-scale circulation and station rainfall corresponding to this SVD mode, we designed composite maps of rainfall, for SLP and 850hPa wind. Based on the SVD expansion coefficients, the years of 1984, 1986, 1990, 1997 and 2000 are selected as wet years, whereas 1988, 1993, 1995 and 2003 are selected as dry years. A dry-minus-wet composite map is shown in Figure 4. It can be seen that, when dry condition prevails, there is an anomalous anticyclone over a broad region in the western Pacific, covering Taiwan. A triple pattern can be clearly seen in the SLP composite, with consistent low-level circulation anomalies. Note that the anomalous wind field is strikingly similar to that associated with the positive phase of the dominant rainfall pattern in the EASM region studied by Hsu and Lin (2007).

3.2. Relationship with model variables

The relationship between station precipitation and large-scale circulation features in models is now presented. Figures 5 and 6 show the spatial patterns of station precipitation and circulation variables associated with their leading SVD modes for each model. It is encouraging that the model Z500 features are consistent with those to be obtained from observation (see Figure 5). In particular, there is a broad-scale positive anomaly in the western Pacific, covering Taiwan, and a negative signal is found near Japan. Accompanying these is reduced rainfall over the northern part of Taiwan, which is in agreement with observation. However, details of the Z500 pattern vary from one model to another. For example, the positive signal north of Japan (see Figure 3b) is absent in HMC and NCEP models, while it is shifted westward for JMA. The negative center over Japan and the Korea peninsula found in observation is

located too far north in the METRI counterpart. When compared with the observational result (see Figure 3c), the correlation between expansion coefficients of station precipitation and Z500 is relatively low for JMA, METRI, and NCEP data. For CWB, HMC, and MGO, the correlation coefficient is comparable to the case in observation (~0.6).

Figure 6 gives the first SVD mode using SLP and station precipitation from each model as input. In broad agreement with observation, most model SLP patterns show a positive anomaly over the western Pacific, and a negative anomaly at 30°-40°N. However, details of the tripole feature of the observed anomalies SLP are not well captured in every model. For instance, a northward shift or expansion of the negative anomaly is found in HMC and NCEP. The negative center of action near Japan is weakened or even absent for CWB and JMA. For the correlation between expansion coefficients of precipitation and SLP, those from JMA, METRI, MGO and NCEP are relatively low, while those from CWB and HMC are comparable to the observational value.

In summary, the spatial patterns for the leading SVD modes between large-scale variables (Z500 and SLP) and station precipitation for most models resemble their respective observational counterpart. From the model hindcast datasets, the prominent signal of the fact that the anomalies are high over the western Pacific and low over Japan is associated with suppressed rainfall in northern Taiwan. However, a number of models seem to have difficulty in capturing the high pressure center over the Sea of Okhotsk. It is also noteworthy that the correlation between the expansion coefficients for the rainfall and Z500 (SLP) fields is especially low for some models runs (~0.36 compared with ~0.6 in observations). In other words, the large-scale circulation features in these GCMs seem to be loosely coupled with station rainfall variability. As

will be seen in the next section, this weak coupling might lead to a low skill in the downscaled rainfall prediction based on these models.

3.3 Downscaling prediction of station rainfall

We now compare the results of precipitation predictions based on raw model outputs and those from downscaling. Figure 7 shows the temporal correlation between model simulated precipitation and observational records for each station location during JJA. It can be seen that most models show no skill in predicting station rainfall. The correlation between the rainfall averaged over all stations in northern Taiwan and that from simulation is negative for every model. After the Multi-Model Ensemble (MME) mean (i.e. simple average of outputs from all models) is taken, the correlation coefficient for the averaged precipitation of the six stations is -0.2.

On the other hand, downscaled products using model output show considerably the skill in predicting station-scale precipitation. Figure 8 gives the correlation between observed rainfall and downscaling prediction using Z500 as a predictor. There is evidence of great improvement of prediction skill. The correlation is positive between northern Taiwan averaged precipitation and the downscaled output for every model. In particular, predictions based on CWB, HMC and JMA give positive skill scores for every station. As for the MME mean of downscaled outputs, the six-station averaged skill score is 0.49.

When we compare Figure 5 with Figure 8, it can be seen that hindcasts from CWB, HMC and MGO give the highest correlation between expansion coefficients of rainfall and model Z500 patterns for their leading SVD modes. The downscaled predictions from these three models also show the highest skill scores. Thus there is a strong association between station rainfall and the model Z500 field. Such a strong relationship, which is similar to that found in observation, leads to a good prediction

of local precipitation using model large-scale variables.

The skill score for downscaled outputs using SLP as a predictor is given in Figure 9. High skill scores are found for downscaled precipitation from CWB, HMC, and JMA hindcasts, and also for that based on MME average. Again, there is relatively high correlation between SVD expansion coefficients for precipitation and SLP for those models with skillful downscaling prediction. The only exception seems to be MGO hindcasts when SLP is used as a predictor. While the temporal correlation is high between the expansion coefficients of SLP and rainfall, downscaling using MGO outputs is not particularly skillful. One possible reason for this could be found upon closer inspection of the SLP pattern corresponding to the first SVD mode (see Figure 6). It shows a negative SLP anomaly over Taiwan, which is opposed to the positive center over the same region in observation (see Figure 3). The erroneous circulation in the leading mode of SLP thus captured could deteriorate the skill of downscaled prediction from this model.

After examining the skill of downscaling based on each predictor, the results using two predictors are shown in Figure 10. For each model, downscaling is carried out by using Z500 and SLP separately, and the final prediction is the simple average of the two downscaled products. Compared with prediction based on a single predictor (see Figures 8 and 9), the prediction based on the downscaled output involving two predictors gives a better performance for the area-averaged precipitation.

Finally, we compare the observed precipitation to predictions based on various methods, on a year-to-year basis. Figure 11 shows the observation, MME average of raw model output, downscaled prediction using Z500, SLP, and Z500 and SLP together. Note that the raw MME output has been rescaled by the ratio of the standard deviation of the observed precipitation to that from simulations. It is immediately

obvious that the model rainfall and the observational record tend to have the opposite sign. On the other hand, downscaling can correct the sign of rainfall prediction. For example, during 1983-87, 1989, 1990, 1997, 1998, and 2002, downscaled results give the same sign as the observed station precipitation, while the model output and observation are out of phase. For the year of 1998, downscaling successfully predicts the sign of rainfall anomaly, but its amplitude is too strong when compared with that found in station data. It is possible that the model response is overestimated in this strong La Nina year. The method of downscaling successfully corrects the sign of prediction but fails to correct its amplitude. Results from Figure 11 also suggest that downscaling based on Z500 and SLP together gives a stable and skillful prediction. Overall, our study demonstrates that downscaled precipitation based on large-scale variables from GCMs is useful in regional climate prediction, which corroborates coarse-resolution forecast products from global climate models.

4. Summary and discussion

In this study, statistical downscaling based on GCM outputs of large-scale circulation variables is used to predict station rainfall over northern Taiwan. In particular, Z500 and SLP from 6 different global models are used as predictors. Downscaling is shown to considerably outperform global models in predicting regional precipitation. In general, downscaling predictions using Z500 give higher scores than those based on SLP as a predictor. This may be due to the inability on the part of some GCMs to represent a realistic coupled pattern between SLP and station precipitation. On the other hand, the Z500 pattern coupled to station rainfall seems to be better captured in models. Also, it is shown that the mean of downscaling results based Z500 and SLP gives a more stable and skillful prediction. Overall, statistical downscaling can be a powerful method in extracting useful information on local

climate variation from GCM outputs.

Our results also suggest that the skill of downscaling is closely related to the following factors. (1) The ability of GCMs in capturing the coupled pattern between predictor and predictand: For example, for the JMA hindcast data, SLP (which is relatively well captured) can be regarded to be a better predictor when compared with Z500. (2) The degree of coupling between a model predictor and the predictand in the temporal sense: For instance, downscaling using NCEP data gives a poor skill. This may be related to the low correlation between the model large-scale circulation pattern and station rainfall, even though the model coupled patterns are realistic.

In the present study, the downscaling based on a single predictor (Z500 or SLP) is investigated. Further investigation of downscaling based on multiple predictors will be carried out in the future.

Acknowledgment. The authors thank the Central Weather Bureau for providing the station data of precipitation. The authors also appreciate those institutes participating in the APCC multi-model ensemble operational system for providing the hindcast experiment data. Also we thank Saji Njarackalazhikam Hameed, Ashok Karumuri, Mong-Ming Lu, Shu-Ping Weng, and Jyh-Wen Hwu for giving valuable comments on this study. The assistance from Doo-Young Lee, Daisuke Nohara, and Bong-Geun Song for data analysis is also appreciated.

References

Benestad, R. E. (2004), Empirical-statistical downscaling in climate modeling, *Eos Trans. AGU, 85(42)*, 417 422, doi:10.1029/2004EO420002.

Díez, E., C. Primo, J. A. García-Moya, J. M. Gutiérrez, and B. Orfila (2005), Statistical and dynamical downscaling of precipitation over Spain from DEMETER seasonal forecasts, *Tellus, Ser. A., 57*(3), 409 423, doi:10.1111/j.1600-0870.2005.00130.x

Feddersen H, A. Navarra, and M. N. Ward (1999), Reduction of model systematic error by statistical correction for dynamical seasonal predictions, *J. Climate* , *12*,1974 1989, doi: 10.1175/1520-0442(1999)012<1974:ROMSEB>2.0.CO;2

——, Andersen U. (2005), A method for statistical downscaling of seasonal ensemble predictions, *Tellus, Ser. A., 57*, 398 408, doi:10.1111/j.1600-0870.2005.00102.x

Giorgi, F., and Coauthors (2001), Regional climate simulation—Evaluation and projections, Climate Change 2001: The Scientific Basis, J. T. Houghton et al., Eds., *Cambridge University Press*, 944 pp.

Grotch, S.L., and M. MacCracken (1991), The use of general circulation models to predict regional climate change, *J. Climate, 4,* 286 303, doi:10.1175/1520-0442(1991)004<0286:TUOGCM>2.0.CO;2

Hsu, H.-H., and S-M. Lin (2007), Asymmetry of the tripole rainfall pattern during the East Asian summer, *J. Climate, 20,* 4443-4458, doi:10.1175/JCLI4246.1.

Kang, I.-S., and Coauthors (2002), Intercomparison of the climatological variations of Asian summer monsoon precipitation simulated by 10 GCMs, *Climate Dyn., 19*, 383 395, doi:10.1007/s00382-002-0245-9.

——, and J.-Y. Lee, and Chung-Kyu Park (2004), Potential predictability of summer mean precipitation in a dynamical seasonal prediction system with systematic

error correction, *J. Climate, 17*, 834-844, doi: 10.1175/1520-0442 (2004) 017 <0834:PPOSMP>2.0.CO;2

Kang, H., K.-H. An, C.-K. Park, A. L. S. Solis, and K. S. (2007), Multi-model output Sstatistical downscaling prediction of precipitation in the Philippines and Thailand, *Geophys. Res. Lett., 34*, L15710, doi:10.1029/2007GL030730.

Kim, M.-K., I.-S. Kang, C.-K. Park , and K.-M. Kim (2004), Superensemble prediction of regional precipitation over Korea, *International Journal of Climatology, 24*, 777 790, doi:10.1002/joc.1029.

Lau, N.-C. (1985), Modeling the seasonal dependence of the atmospheric response to observed El-Nino in 1962 76. *Monthly Weather Review 113*,1970 1996, doi:10.1175/1520-0493(1985)113<1970:MTSDOT>2.0.CO;2.

Murphy, J. (1999), An evaluation of statistical and dynamical techniques for downscaling local climate, *J. Climate, 12,* 2256-2248, doi:10.1175/1520-0442(1999)012<2256:AEOSAD>2.0.CO;2.

Rowell, D. P. (1998), Assessing potential seasonal predictability with an ensemble of multidecadal GCM simulations, *J. Climate, 11*, 109-120, doi:10.1175/1520-0442(1998)011<0109:APSPWA>2.0.CO;2.

Sperber, K. R., and T. N. Palmer, (1996), Interannual tropical rainfall variability in general circulation model simulations associated with the Atmosphere Model Intercomparison Project. *J. Climate, 9,* 2727 2750, doi:10.1175/1520-0442(1996)009<2727:ITRVIG>2.0.CO;2.

——, and Coauthors (2001), Dynamical seasonal predictability of the Asian summer monsoon. *Mon. Wea. Rev., 129,* 2226 2247, doi:10.1175/1520-0493(2001)129<2226:DSPOTA>2.0.CO;2.

Von Storch H, Zorita E, Cubasch E. (1993), Downscaling of global climate estimates

to regional scales: an application to the Iberian rainfall in wintertime, *J. Climate, 6*, 1161-1171, doi: 10.1175/1520-0442(1993)006<1161:DOGCCE>2.0.CO;2.

——, and F. W. Zwiers (1999), Statistical Analysis in Climate Research, *Cambridge University Press*, 484.

Wang, W.-C., H.-H. Hsu, W.-S. Kau, X.-Z. Liang, LinHo, C.-T. Chen, A. N. Samel, C.-H. Tsou, P.-H. Lin, and K.-C. Ko, (1998), GCM simulations of the east Asia climate. 473-482. Proceedings of the Third East Asia-West Pacific Meteorology and Climate Conference, (Ed.) C.-P. Chang, *World Scientific Publication, Corp.* pp562.

Wetterhall, F., S. Halldin, and C.-Y. Xu (2005), Statistical precipitation downscaling in central Sweden with the Analogue Method, *J. Hydrol., 306*, 174 190, doi:10.1016/j.jhydrol.2004.09.008.

Wilby, R.L., T.M.L. Wigley, D. Conway, P. H. Jones, B. C. Hewitson, J. Main, and D. S. Wilks (1998), Statistical downscaling of general circulation model output: A comparison of methods, *Water Resour. Res., 34*, 2995 3008, doi:10.1029/98WR02577

——, Hay, L. E. Hay, and G. H. Leavesley (1999), A comparison of downscaled and raw GCM output: implications for climate change scenarios in the San Juan River Basin, Colorado, *Journal of Hydrology, 225*, 67 91, doi:10.1016/S0022-1694(99)00136-5

Xu, C.-Y. (1999), From GCMs to river flow: a review of downscaling methods and hydrologic modeling approaches, *Progress in Physical Geography, 23*, 229-249.

List of Table Title

Table 1. Description of the GCMs used in this study

List of Figure Caption

Figure 1. The location of the six stations in northern Taiwan considered in this study.

Figure 2. (a) Spatial pattern of the first EOF for station precipitation in northern Taiwan during JJA, for the period of 1951-2006. (b)The principal component of the leading EOF.

Figure 3. The leading SVD mode spatial patterns of (a) the observed station precipitation in northern Taiwan and (b) the observed Z500 in East Asia during JJA. (c) Normalized expansion coefficients corresponding to precipitation and Z500. The leading SVD spatial patterns of (d) the observed station precipitation and (e) the observed SLP in East Asia during JJA. (f) Normalized expansion coefficients for precipitation and SLP (Dotted contours represent negative values in (b) and (e)). Data for the period of 1983-2003 are used.

Figure 4. Dry-minus-wet composites of (a) station precipitation (unit: mm/day), (b) observed SLP field (contours in interval of 0.3mb), and (c) observed 850hPa wind field (unit for scale arrow: 3m/s) during JJA. (wet years: 1984, 1986, 1990, 1997 and 2000; dry years: 1988, 1993, 1995 and 2003)

Figure 5. The leading SVD patterns of (a), (d), (g), (j), (m), (p) the observed station precipitation in northern Taiwan, (b), (e), (h), (k), (n), (q) model Z500, and (c), (f), (i), (l), (o), (r) expansion coefficients for precipitation and Z500 based on CWB((a),(b)), HMC((d),(e)), JMA((g),(h)), METRI((j),(k)), MGO((m),(n)), NCEP((p),(q)) hindcast data during JJA for the period of 1983-2003.

Figure 6. Same as Figure 5, but for station precipitation and model SLP.

Figure 7. The correlation coefficients between the observed JJA station precipitation and precipitation from (a) CWB, (b) HMC, (c) JMA, (d) METRI, (e) MGO, (f) NCEP model, and (g) MME average of model output. Numbers on the horizontal axes represent stations located at Tanshui, Anpu, Taipei, Chutzehu, Ilan and Hsinchu. Correlation coefficients between the average precipitation for all stations and the corresponding mean precipitation from models are given at the top left of each panel.

Figure 8. Same as Figure7, but for the downscaling result using model Z500 output as a predictor.

Figure 9. Same as Figure7, but for the downscaling result using model SLP output as a predictor.

Figure 10. Same as Figure7, but for the downscaling result using model SLP and Z500 output as predictors.

Figure 11. JJA precipitation, averaged over all stations (black), and the corresponding prediction based on different prediction schemes, for the period of 1983-2003 (blue: MME model output, yellow: downscaling prediction based on Z500, green: downscaling based on SLP, red: average of downscaling using Z500 and SLP.). Downscaling results are obtained from averages of downscaled prediction based on individual models. (Unit: mm/day)

Table 1. Description of hindcast experiments used in this study

Acronyms	Institution	Model Resolution	Data Type
CWB	Central Weather Bureau	T42 L18	SMIP/HFP
HMC	Hydrometeorological Centre of Russia	1.12°x1.4° L28	SMIP/HFP
JMA	Japan Meteorological Agency	T63 L40	SMIP/HFP
METRI	Meteorological Research Institute	4°x5° L17	SMIP/HFP
MGO	Main Geophysical Observatory	T42 L14	SMIP/HFP
NCEP	National Centers for Environmental Prediction (a Coupled Forecast system)	T62 L64	CMIP/HFP

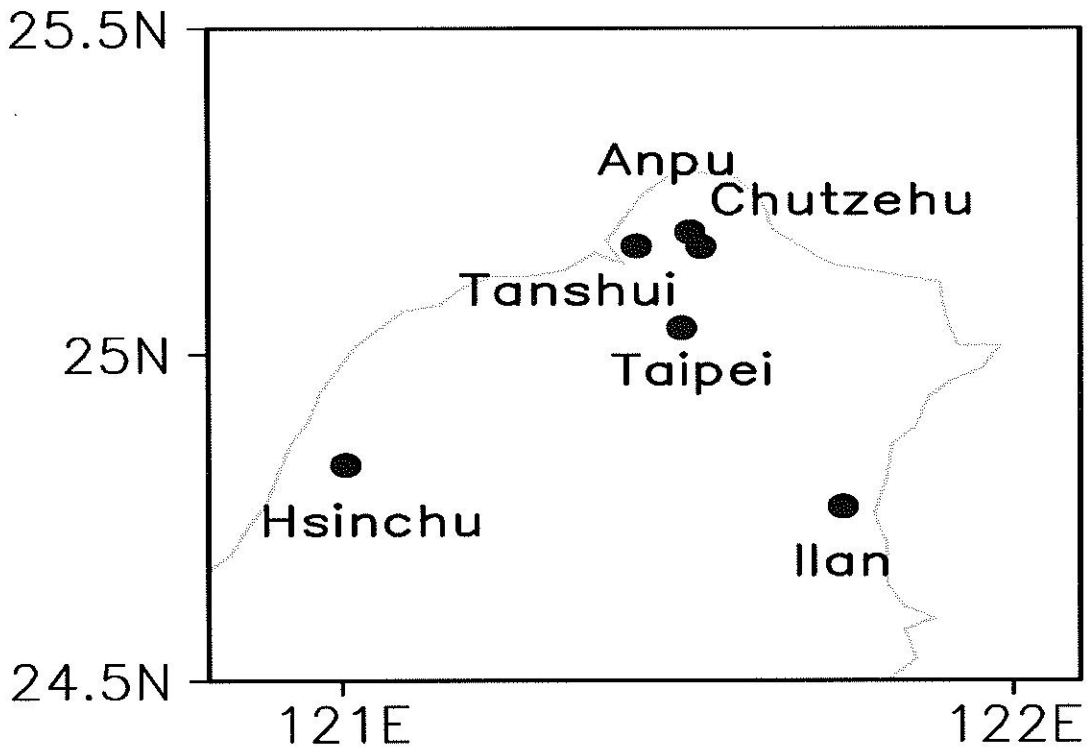

Figure 1. The location of the six stations in northern Taiwan considered in this study.

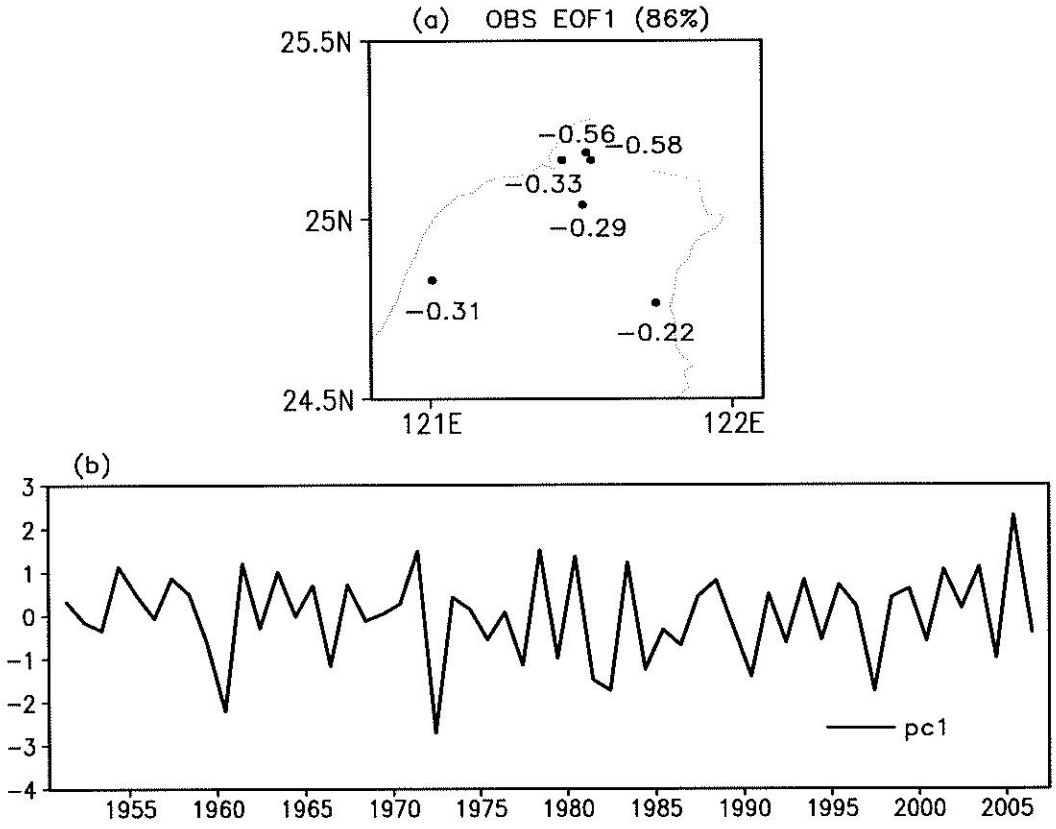

Figure 2. (a) Spatial pattern of the first EOF for station precipitation in northern Taiwan during JJA, for the period of 1951-2006. (b)The principal component of the leading EOF.

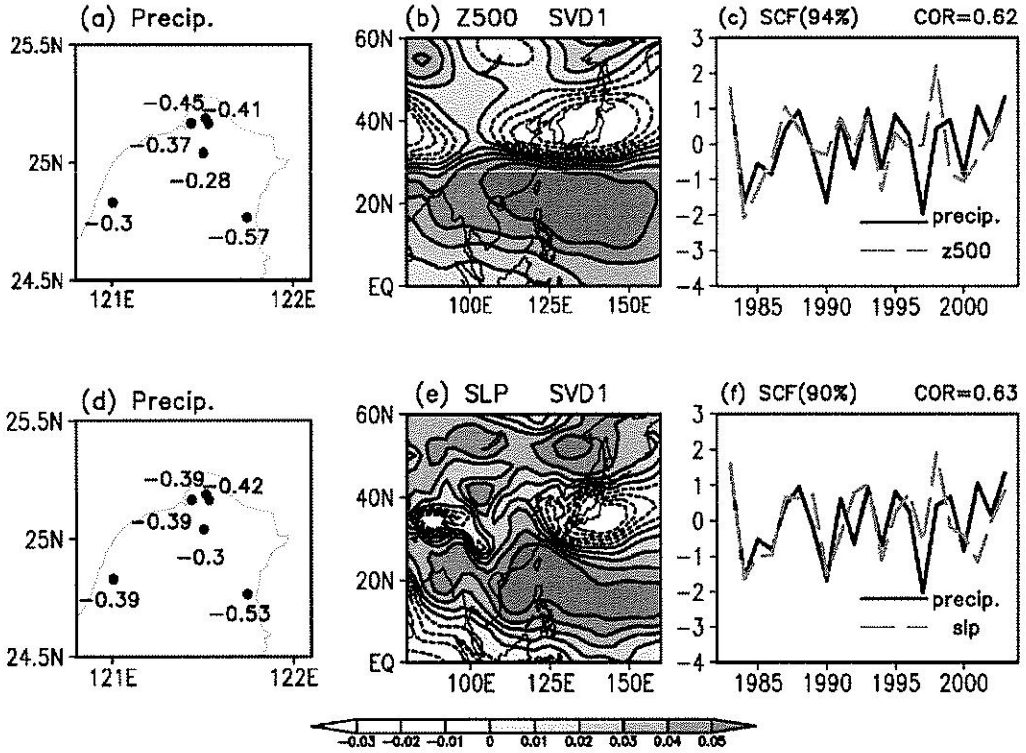

Figure 3. The leading SVD mode spatial patterns of (a) the observed station precipitation in northern Taiwan and (b) the observed Z500 in East Asia during JJA. (c) Normalized expansion coefficients corresponding to precipitation and Z500. The leading SVD spatial patterns of (d) the observed station precipitation and (e) the observed SLP in East Asia during JJA. (f) Normalized expansion coefficients for precipitation and SLP (Dotted contours represent negative values in (b) and (e)). Data for the period of 1983-2003 are used.

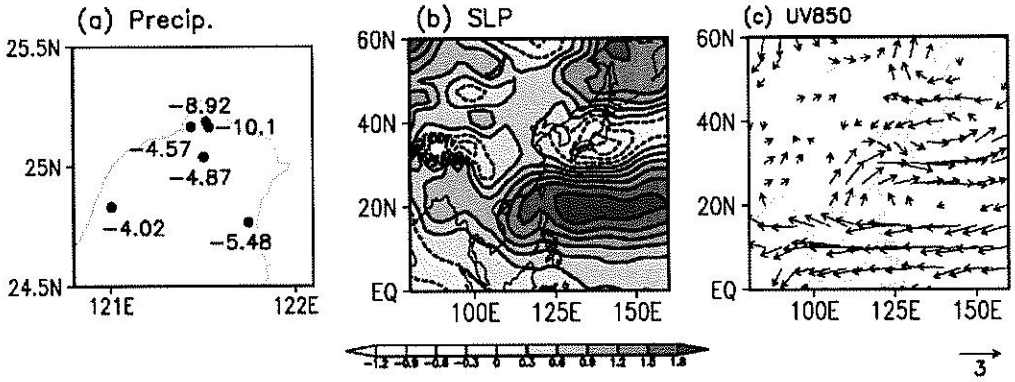

455 Figure 4. Dry-minus-wet composites of (a) station precipitation (unit: mm/day), (b) observed SLP field (contours in interval of 0.3mb), and (c) observed 850hPa wind field (unit for scale arrow: 3m/s) during JJA. (wet years: 1984, 1986, 1990, 1997 and 2000; dry years: 1988, 1993, 1995 and 2003)

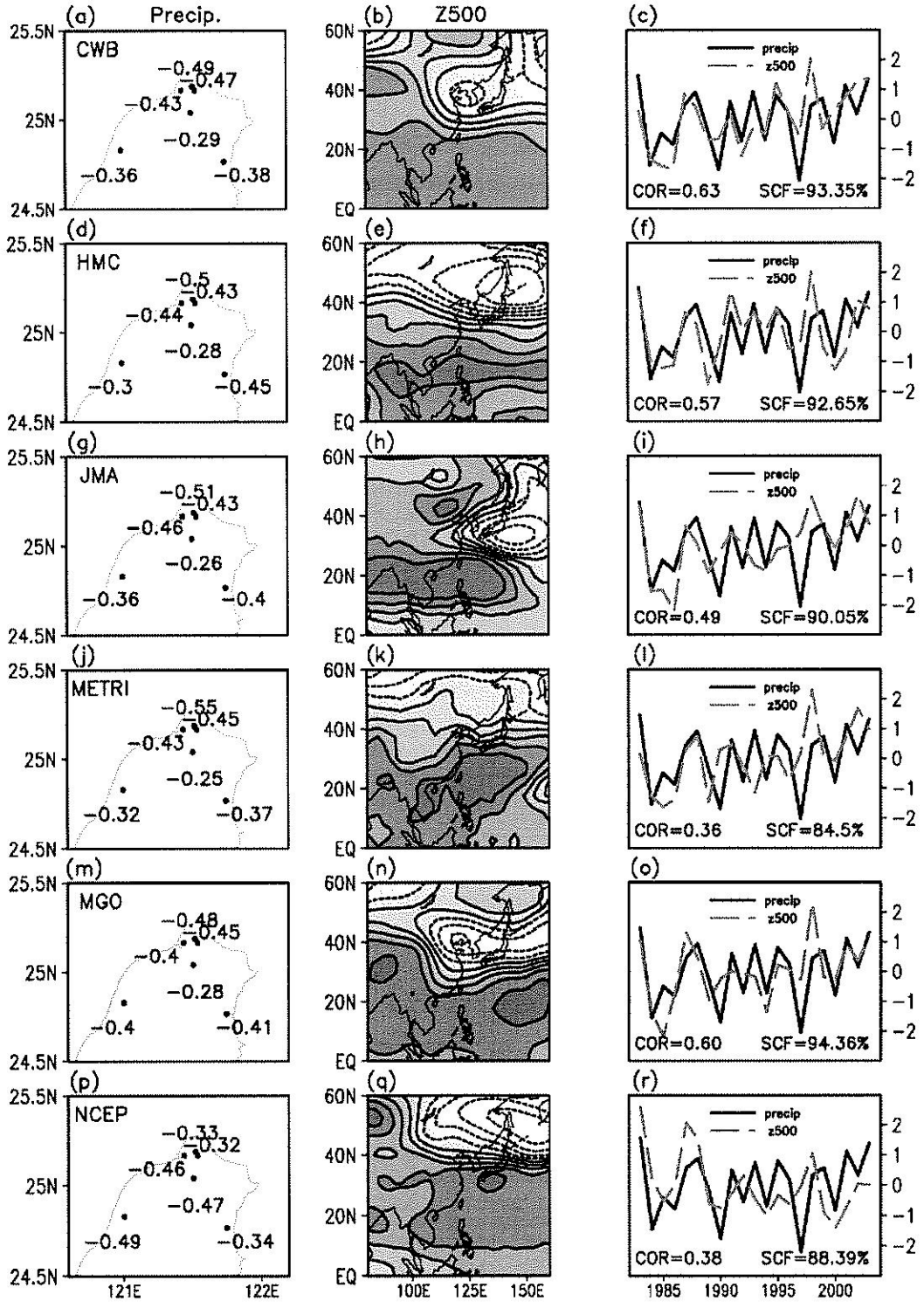

460 Figure 5. The leading SVD patterns of (a), (d), (g), (j), (m), (p) the observed station precipitation in northern Taiwan, (b), (e), (h), (k), (n), (q) model Z500, and (c), (f), (i), (l), (o), (r) expansion coefficients for precipitation and Z500 based on CWB((a),(b)), HMC((d),(e)), JMA((g),(h)), METRI((j),(k)), MGO((m),(n)), NCEP((p),(q)) hindcast

data during JJA for the period of 1983-2003.

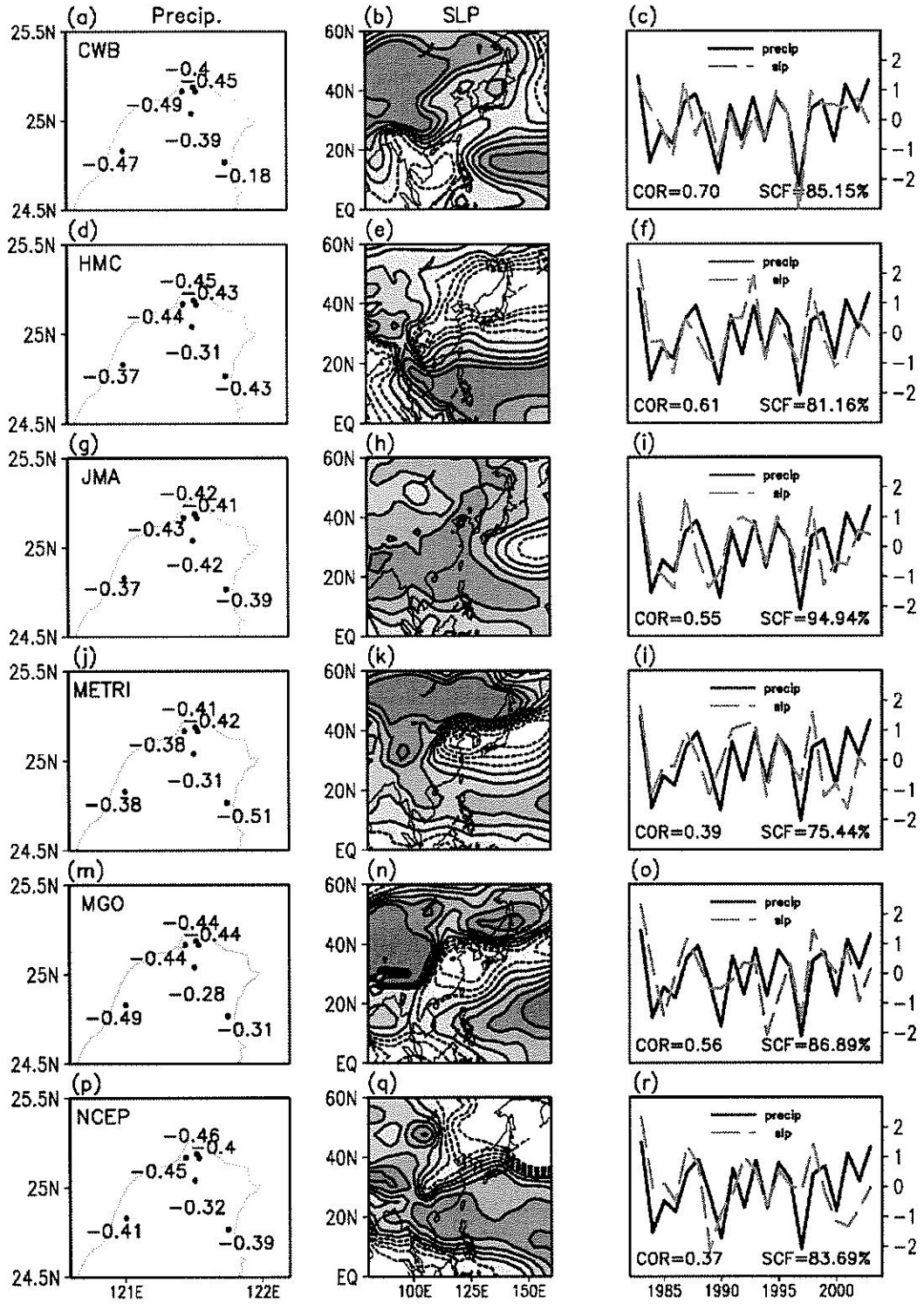

Figure 6. Same as Figure 5, but for station precipitation and model SLP.

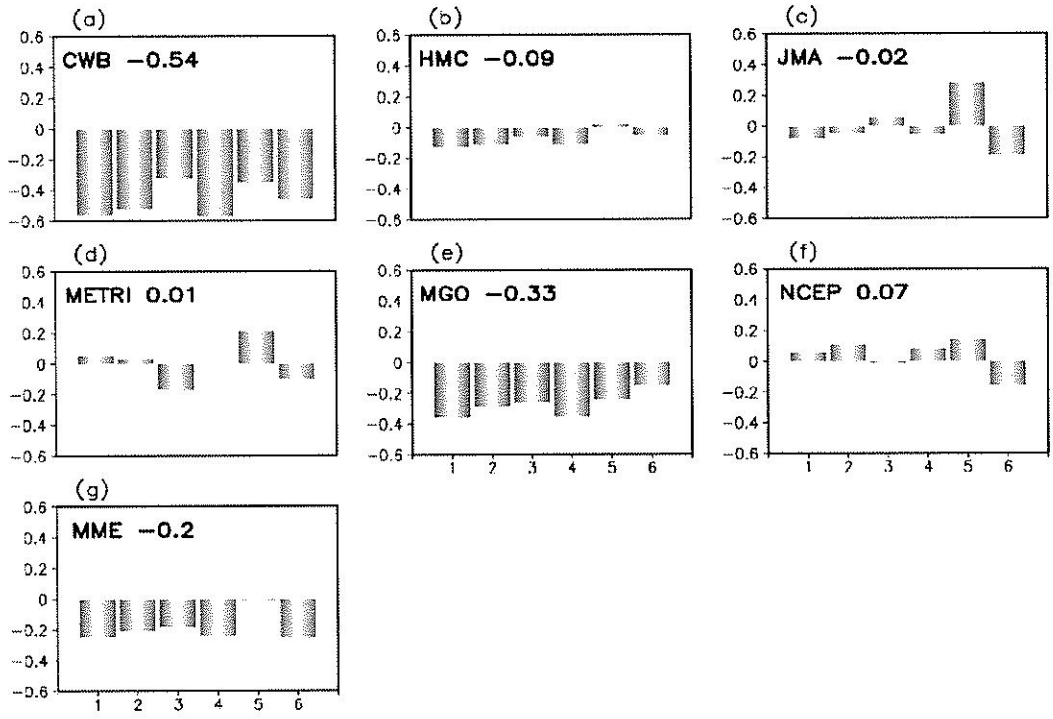

Figure 7. The correlation coefficients between the observed JJA station precipitation and precipitation from (a) CWB, (b) HMC, (c) JMA, (d) METRI, (e) MGO, (f) NCEP model, and (g) MME average of model output. The numbers on the horizontal axes represent stations located at Tanshui, Anpu, Taipei, Chutzehu, Ilan and Hsinchu. The correlation coefficients between the average precipitation for all stations and the corresponding mean precipitation from models are given at the top left of each panel.

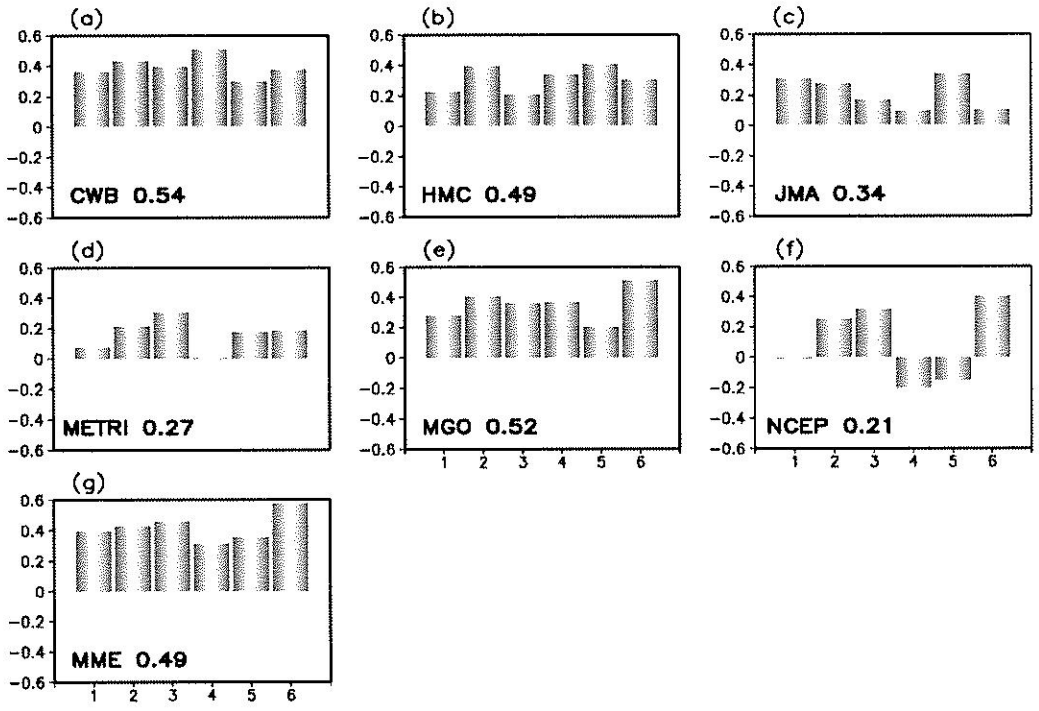

475 Figure 8. Same as Figure7, but for the downscaling result using model Z500 output as a predictor.

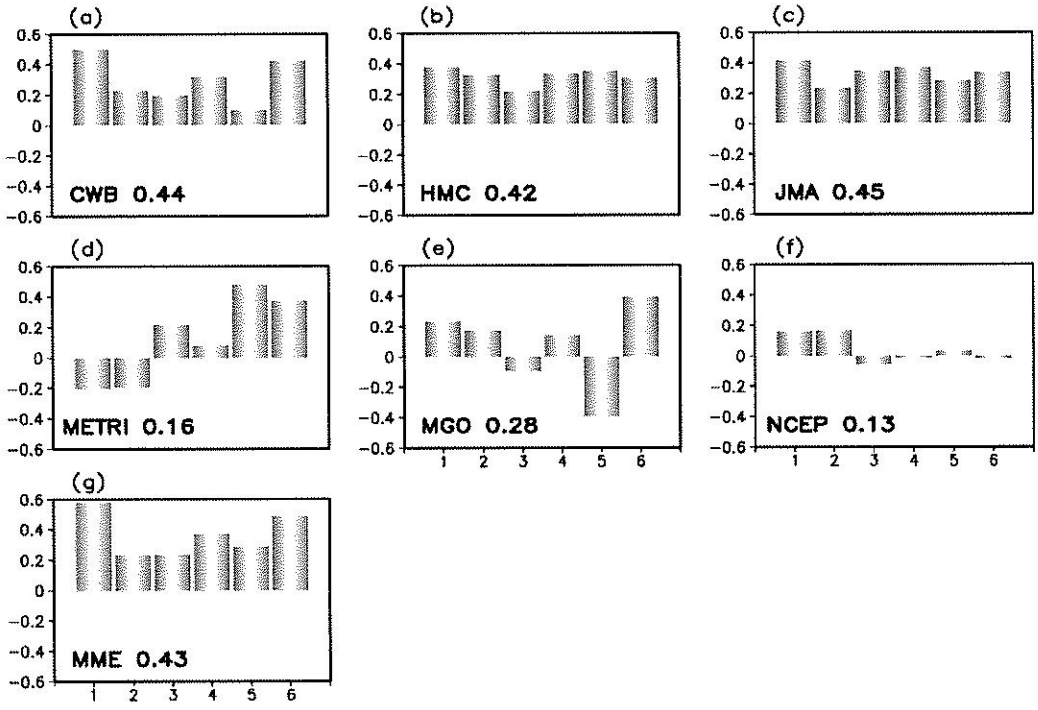

Figure 9. Same as Figure7, but for the downscaling result using model SLP output as a predictor.

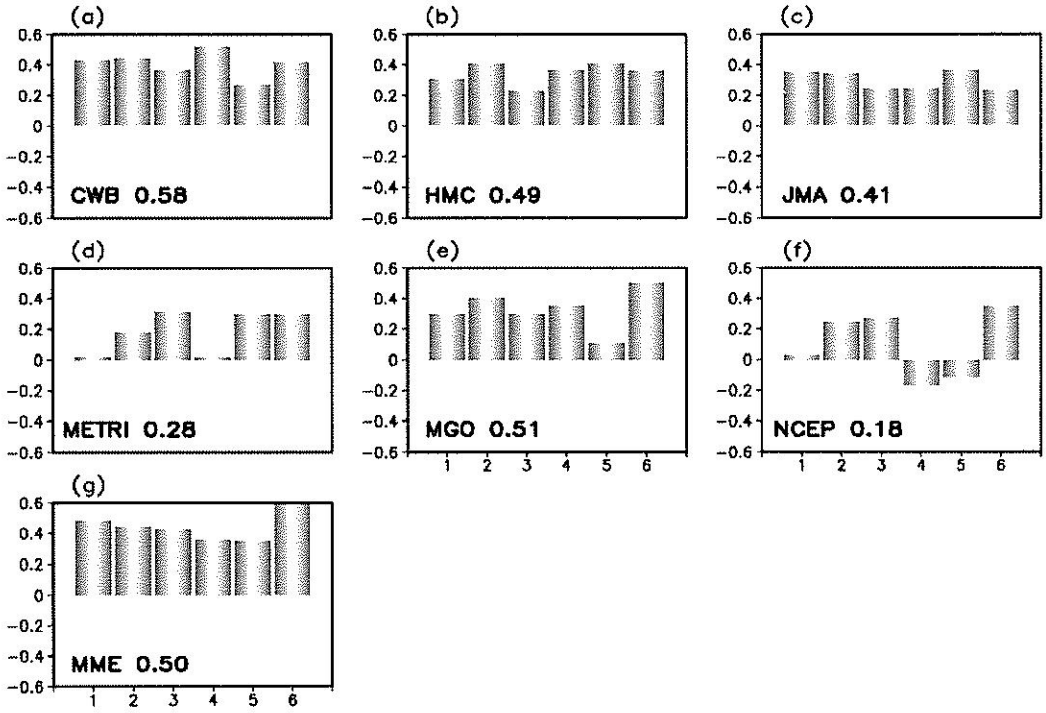

Figure 10. Same as Figure7, but for the downscaling result using model SLP and Z500 output as predictors.

485

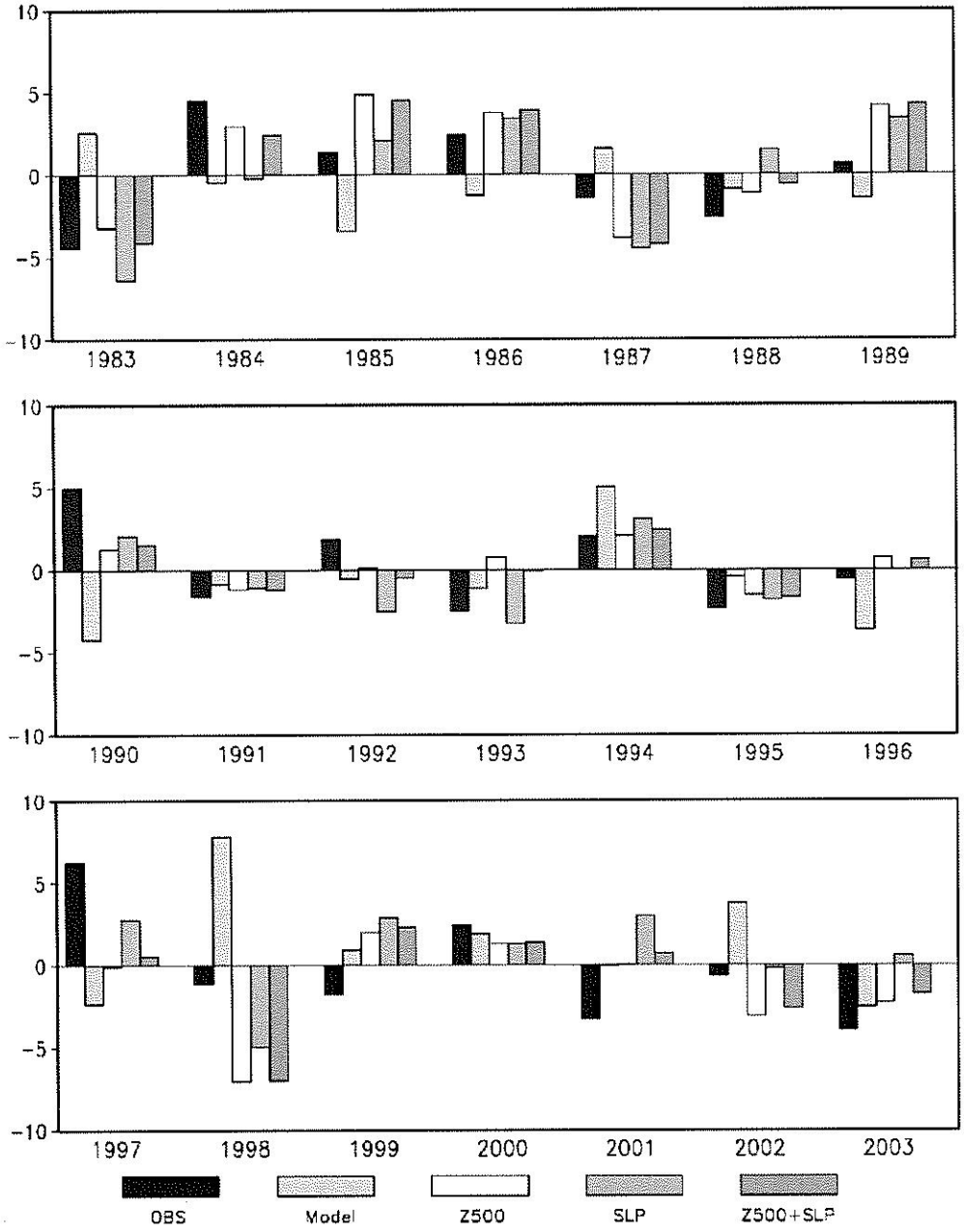

Figure 11. JJA precipitation, averaged over all stations (black), and the corresponding prediction based on different prediction schemes, for the period of 1983-2003 (blue: MME model output, yellow: downscaling prediction based on Z500, green: downscaling based on SLP, red: average of downscaling using Z500 and SLP.). Downscaling results are obtained from averages of downscaled prediction based on individual models. (Unit: mm/day)